Back to Session Subjects

Recent Progress on the Development of a Smart Rotor System

Inderjit Chopra

Alfred Gessow Professor & Director
Alfred Gessow Rotorcraft Center
Department of Aerospace Engineering
University of Maryland, College Park, MD 20742, USA

Abstract

This paper reviews the status of smart structures technology development for application to rotorcraft systems. Though a large component of research is focused to the minimization of helicopter vibration, the methodology is equally applicable to other problems such as aeromechanical stability augmentation, handling qualities enhancement, stall alleviation, reduction of interior/exterior acoustic signatures, minimization of blade dynamic stresses and rotor head health monitoring. More than any other system, the structural, mechanical and aerodynamic complexity and the interdisciplinary nature of rotorcraft offer many opportunities for the application of smart structures technologies with the potential for substantial payoffs in system effectiveness. Primarily, two types of smart rotor concepts are under development: trailing-edge flaps actuated with smart actuators, and controllable twist blades with embedded piezoceramic actuators. For flap actuation, actuators range from piezo-bimorphs, piezo/electrostrictive stacks and piezo/magneto-strictive-induced composite-coupled actuation. Most smart actuators are moderate force and extremely small displacement devices and hence some form of mechanical amplification of induced displacement is needed to achieve desired flap deflections. Because of compactness and weight considerations, the stroke amplification of these devices has been a key barrier for application to rotor blades. Most of the current smart rotor models under development have adopted the Froude scaling, but future developments are tending towards the Mach-scale and full-scale designs. The state-of-art on modeling of actuators is improving rapidly. Shape memory alloys (SMA) show potential of providing large induced strains (up to 6%), but are limited to low frequency (less than 1 Hz) applications such as tab adjustment for rotor tracking. Also, it is quite difficult to achieve fine-tune actuation control with SMA. Data base of smart actuators' characteristics under different loads, frequency and temperature are non-existent. For in-flight tracking of rotor SMA-actuated tab, it is important to incorporate adaptive control strategy and a locking mechanism. Comprehensive rotor analyses covering smart materials actuators are in development at this time. This paper will identify key barriers for applications of smart structure technology to rotorcraft systems and point out the need for future research in this area. The research in the application of smart structures technology to rotorcraft systems is in its early phase and activities need to be expanded before this promising technology can be exploited in a competitive manner.

1. Introduction

Helicopters are susceptible to high vibratory loads, excessive noise levels, aeromechanical instabilities, poor flight stability characteristics, and high dynamic stresses. Compared to fixed-wing aircraft, helicopters suffer from high operating cost, poor ride quality, low fatigue life of structural components, inferior handling qualities and a restricted flight envelope. To reduce these problems to an acceptable level, numerous passive and active devices, and many ad hoc design fixes, are resorted to with resultant weight penalties and reduced payloads. The primary source for all these problems is the nonsteady and complex aerodynamic environment in which the rotor must operate and the complex coupled structural and mechanical system comprised by the rotor, body, transmission system and engine. To counter some of these deficiencies, and also to further expand the flight capabilities of military and civilian helicopters, many new design modifications and devices are being contemplated. These appear to show incremental and modest gains in terms of performance improvement and reduction in operating costs. If the objective is to achieve '*a jet smooth ride*' with helicopters at a comparable operating cost, for example, one has to try revolutionary ideas. One innovative idea that appears to show the potential for a significant gain in performance improvement at a small penalty is to apply the technology of smart structures to rotorcraft. For such an application, numerous light-weight sensors and actuators are embedded or surface-mounted at different stations on the blades, and optimal distributed forces applied with the help of modern control theory.

At this time, smart structures technology is in its early stage of development, and its applications to various physical systems are evolving to actively control vibration, noise, aeromechanical stability (damping), shape and stress distribution. This paper

will review the state-of-the-art on the application of smart structures technology to rotor systems.

1.1 Smart Structures

A smart structure involves distributed actuators and sensors, and one or more microprocessors that analyze the responses from the sensors and use distributed-parameter control theory to command the actuators to induce localized strains/displacements to minimize response or loads at selected stations. A smart structure has the capability to respond to a changing external environment (such as loads and shape change) as well as to a changing internal environment (such as damage or failure). It incorporates actuators that allow the alteration of system characteristics (such as stiffness or damping) as well as of system response (such as strain or shape) in a controlled manner [1]. Many types of actuators and sensors are being considered, such as piezoelectric materials, shape memory alloys, electrostrictive materials, magnetostrictive materials, electro-rheological/magneto-rheological fluids and fiber optics. Typically, these can be integrated with main load-carrying structures by surface bonding or embedding without causing any significant changes in the structural stiffness of the system. Among these, piezoelectrics are the most common. They undergo strain (elongation) when an electric field is applied across them and produce voltage when strain is induced, and thus can be used both as actuators and sensors. These materials, however, generate very low strains but over a wide range of actuation frequency. The most widely used piezoceramics (such as lead zirconate titanate: PZT) are in the form of thin sheets which can be readily embedded or attached to composite structures [2,3].

Among other materials, shape memory alloys (SMA) are gaining rapid recognition as actuators because of the possibility of achieving large excitation forces and displacements. These alloys undergo phase transformation at a specific temperature. When plastically deformed at a low temperature, these alloys recover to their original undeformed condition if the temperature is raised above the transformation temperature. This process is reversible. The most common SMA material is Nitinol (nickel titanium alloy) and is available in the form of wires of different diameters. Though heating can be carried out internally (electrically), response is very slow (about 1 Hz). The thermo-mechanical behavior of SMA depends upon the internal crystalline structure (phase), temperature, stress, strain rate, and history of the material. The material resides in the austenite phase at higher temperatures and the Young's modulus of SMA in this phase is much higher (3-5 times) than the modulus in the martensite phase (at low temperatures) [4,5].

Electrostrictive materials are similar to piezoelectric materials, with slightly better strain capability, but are very sensitive to temperature [6]. Magnetostrictive materials such as Terfenol-D elongate when exposed to a magnetic field. These materials generate low strains and moderate forces over a wide frequency range. Because of coil and magnetic return path, these actuators are often bulky [7]. Fiber optics are becoming popular as sensors because they can be easily embedded in composite structures with a negligible effect on the structural integrity and also have the potential of multi-plexing [8]. Piezoelectric and electrostrictive materials are also available in the form of 'stacks' where many layers of materials and electrodes are assembled together. These stacks generate large forces but small displacements, in the direction normal to the top and bottom surface [9]. Also, piezoceramics in form of bimorphs or bending actuators are available commercially where two layers of these materials are stacked with a thin shim (typically of brass) between them. If an electric field is applied such that one of the piezo layers expands while the other one contracts, a pure bending action results [10].

1.2 Potential Applications to Rotorcraft

The multidisciplinary nature of rotorcraft offers many opportunities for the applications of smart structures technologies with the potential for very substantial payoffs in system effectiveness. The rotor is the key subsystem, setting the current limits on vehicle performance, handling qualities and reliability. The flow field on the rotor disk is extremely complex and may involve transonic flow on the advancing blade tips, dynamic stall and reversed flow on the retreating side of the disk, highly yawed flows on the front and rear part of disk, and blade-vortex interactions. The primary source of helicopter vibration is the main rotor that transmits large vibratory forces and moments to the fuselage. For an N-bladed rotor, the N/rev, N-1/rev and N+1/rev vibratory blade loads (in rotating frame) are transmitted to the body through the hub as dominating N/rev vibratory forces and moments. In contrast to traditional passive devices, active vibration control is achieved through excitation of blade pitch at higher harmonics of the rotational speed, thereby canceling vibratory forces at their source. Blade feathering/twist on the order of 1 to 2 degrees is required to suppress vibrations. Higher Harmonic Control (HHC) systems incorporate excitation of the swashplate at N/rev with servo actuators, and have been widely investigated as a viable concept to suppress vibration through numerical simulations, rotor model tests in wind tunnels and in flight tests [11-14]. Although this active system has been proven to be quite effective in reducing vibration and may incur a lower weight penalty (up to 1-2% of gross weight) than passive systems (weight penalty of 3%), a number of significant drawbacks exist. The power requirements of the servo-actuators needed to excite the swashplate become substantial at extreme flight

conditions, where vibrations are likely to be highest. Also, excitation frequencies of conventional swashplates are restricted to multiples of N/rev. It is well known that other harmonics are important to minimize blade stresses and to improve rotor performance. The limitations of HHC have spurred research on Individual Blade Control (IBC) systems that control pitch of each blade independently with servo-actuators mounted in the rotating frame [15-17]. Although blades can be excited at any desired combination of frequencies, there is a mechanical complexity of hydraulic sliprings. Again, the weight penalty of this system may not be less than an HHC system. To overcome many of these problems associated with existing active control devices, there has been growing interest recently in the application of smart structures technology to rotor systems in order to reduce vibration and noise level as well as to improve rotor performance.

Because the rotor is a flexible structure, changes in shape, mechanical properties and stress/strain fields can be imposed upon it. These in turn will alter the vibratory modes, aeroelastic interactions, aerodynamic properties, and dynamic stresses of the rotor. Smart structures technologies will enable these imposed changes to be tailored to conditions sensed in the rotor itself. Furthermore, because the smart actuators and sensors can be distributed over each individual rotor blade, control can be imposed over a much larger bandwidth than with current swashplate-based controls, which are limited to N/rev for an N-bladed rotor. This opens up a hitherto unavailable domain for vibration control, aeromechanical stability augmentation, handling qualities enhancement, stall alleviation, and acoustic suppression. The use of smart structures also offers the prospect of in-flight tracking of main rotor blades and sensing structural damage in the rotor, drive-train and other critical components. The pilot can then be alerted to take suitable action. A further very promising application of smart structures is to actively control the interior noise of a rotorcraft [18]. Structure-borne noise can be minimized by actively controlling the response of airframe panels. A source of high frequency interior noise can be drive-train system (gearbox meshing tonal frequencies). Actively tuning transmission strut systems with smart actuators may minimize noise in cabin (high frequency noise cancellation) [19].

1.3 State of the Art

Recently, there has been an increase in smart structures research activities, covering a wide range of applications to aerospace, automotive, civil, marine, machine tools and medical fields. Much of the earlier work is focused on the application of piezoelectric technology to space related systems, such as the control of vibration of large space structures [20], and for stable bases for precision pointing in space (telescope, mirrors, etc., see Ref. [21]). Also, there are applications to the field of fixed-wing aircraft, such as controlling wing twist and camber for wing divergence and flutter suppression [22-27], increasing panel flutter boundary [28] and controlling structure-borne noise [29]. Recently, there have been growing research activities on the use of smart structures for rotorcraft applications to actively control vibration and external/internal noise, augment damping and improve rotor performance (see a special issue in *Smart Materials & Structures,* (February 1996) and review articles [30-31]).

Much of the work in this field has focused on building dynamically-scaled smart rotor models [30]. Two types of Froude-scale models have been built: controllable twist models incorporating embedded specially-shaped piezoelectric elements, and trailing-edge flap models actuated by piezoceramic and magnetostrictive actuators. These rotor models were tested in a vacuum chamber, on a hover stand and in a wind tunnel. For both types of models, the performance of the actuation systems degraded dramatically at higher rotational speeds because of higher dynamic pressure, centrifugal force and frictional moments. For trailing-edge flap models, one requires a compact torsional actuation technique and several approaches have been examined to drive the flap. These include piezoceramic elements, piezo-bimorphs, piezostacks and magnetostrictictive actuators in conjunction with either a mechanical amplification arrangement or twist-inducing tailored composite coupling. A mechanical leverage system incorporates moving hinges and often suffers from slippage and frictional moments at joints. On the other hand, tailored extension-twist or bending-twist composite coupling may eliminate moving hinges and also may be able to use the full length of the blade for housing, but often suffer from structural efficiency. For controllable twist models, banks of piezoceramic elements are embedded under the skin at ±45 deg relative to the blade span axis respectively on the top and bottom surfaces; an in-phase activation induces a pure twist in the blade. To induce a sufficient blade twist for active control of vibration or noise, a large number of distributed piezoceramic elements are required that incur a significant weight penalty and an increase in blade stiffness from its baseline value. This scheme affords actuation redundancy and involves no moving hinges, but imposes structural integrity issues. At this stage, even though both type of models have not achieved the desired level of flap deflection or blade twist, they show potential for further improvements.

Straub [32] carried out a feasibility study of using smart structures technology for primary as well as active control of a full-scale vehicle. For this study, the AH-64 helicopter was selected. It was concluded that the concept of twist and camber control using embedded actuators is not practical with the available smart materials. Servoflap control system using on-blade smart material actuators

appeared conceptually feasible for primary and active controls [33]. There are other studies that discuss various applications of smart structures technology to rotorcraft systems [34], including collective pitch control with SMA actuation [35], dynamic stall delay with piezostack actuated leading-edge flaps [36, 37], damping augmentation with electro-rheological and magneto-rheological dampers [38], active transmission mounts with smart actuators to control vibration and noise [39], vibration minimization with active control of structural response (ACSR system) using distributed smart actuators in airframe [40] and active/passive constrained layer damping control of flexbeams [41].

So far there has been limited research towards the development of analytical tools for a smart rotor. Currently most methods are focused to predict the static and dynamic response of non-rotating anisotropic beams that too limited to bending and extension of beams using paired piezo-actuation (via identical actuators bonded to the top and bottom surfaces of the beam) [42, 43]. Continued research in this area is expanding these theories to include the coupled torsion/bending/extension of beams with single or multiple piezo elements not aligned along the beam axis and bonded on one or both surfaces of the beam [44, 45]. Recently, there has been some effort [46] to develop a coupled actuator-flap-rotor dynamic analysis, but it is far from a comprehensive smart rotor analysis.

The objective of this paper is to assess the status of smart structures technology developments for application to the rotor systems. Though a large part of this research is focused on vibration minimization, these developments are equally applicable to other problems. In this paper four different topics are covered: trailing-edge flap concept, controllable blade twist concept, shape memory alloys actuation concept and analytical modeling of smart rotors.

2. Trailing Edge Flaps

2.1 Trailing-Edge Flaps Actuated with Piezo Birmorphs

This section discusses the development of a scaled rotor model with piezo-bimorphs (piezo-benders) actuated trailing edge flaps. The flaps are located near the tip of the blade (Fig. 1). A piezo-bimorph is a bending actuator and consists of piezoceramic (PZT) sheets that are bonded on both sides of a very thin brass shim with an electrically conducting adhesive coating. When the bimorph is clamped at one end, and equal but opposite fields are applied to the PZT sheets, a pure bending of the bimorph occurs. The resulting small tip displacement of the bimorph is amplified using a mechanical leverage or flexure system to provide the actuation stroke for the flap (Figs. 2). The piezo-bimorph is a compact actuation device and generates a small actuation force.

References [46-52] present the development of a six foot diameter, two-bladed, 1/8-th Froude scale bearingless rotor (ITR-Boeing simulation) model with flaps actuated with piezo-benders. Blades were constructed out of rigid foam, covered with fiber-glass prepreg fabric, embedded with a spar made of unidirectional glass-epoxy prepreg. The spar was located near the quarter chord to carry blade centrifugal loads in rotation. To minimize the possibility of aeroelastic instability in rotation, the sectional center of gravity of blades was placed at the quarter-chord by adding tantalum weights near the leading edge. The blade used NACA0012 airfoil sections and was 3.0 inch in chord length. The trailing edge flap consisted of 4.38 inch length, 0.6 inch wide (20% chord) plain flap located at the trailing edge.

Samak [47] first demonstrated the feasibility of using piezo-bimorphs to actuate trailing edge flaps of a rotor model. Commercially available two-layered bimorphs (G-1195) were used to actuate the flaps. The trailing edge flap was actuated by three 1.5 inch long, 1.0 inch wide and .021 inch thick piezoelectric bender elements. These bimorph elements were rigidly anchored to the blade spar so that they formed 1.0 inch long cantilever beams. When actuated, these bimorphs bend upward or downward depending on the applied voltage field and produce force when they are restrained at the tip. The bender elements were connected to the flap through a common hinge. A system of mechanical hinges and linkages were used to amplify the bending of the elements at the tip to cause larger flap rotation (Fig. 2). This flap rotation was measured using a Hall Effect sensor with the flux-inducing permanent magnet mounted along the flap hinge line, which rotates with the flap. A two-bladed rotor model was tested on the hover stand. There was enough oscillatory flap amplitude (±7 deg) in a non-rotating condition, but the amplitude precipitously decreased with higher RPM. At the scaled operating speed of 900 RPM, maximum flap amplitude of ±1 deg was achieved. This fell far short of the targeted amplitude of about ±6 deg at N/rev (where N is number of blades) to suppress vibration completely.

Efforts were then focused to increase oscillatory flap deflection at the operating rotational speed. A major drawback of a two-layered piezo-bimorphs was its inability to generate a high actuation force. To actuate a flap in a rotating environment, sufficient actuation force is needed to overcome aerodynamic, centrifugal and frictional hinge moment. Walz [10] formulated a simple rotor analysis using quasisteady aerodynamics and carried out parametric studies to match the flap moment requirements with the capability of actuators. It was shown that the actuation force of a two-layered bimorph is not sufficient to generate the required flap authority. Four-layered bimorph actuators were built in-house in order to increase their actuation force. Also,

modifications to the mechanical leverage arrangement between actuators and flap were incorporated including a rod-cusp arrangement (Fig. 2). In spite of several modifications and improvements to the flap actuation system, the desired increase in flap performance was not realized. Ben-Zeev [48] built new rotor blades with several modifications to actuation system and tested them in the 10 ft diameter vacuum chamber to isolate the effects of centrifugal loading on the actuator-flap performance. A beam model of the piezo bimorph including propeller moment effect (due to rotation) was formulated. The cause of the reduced flap deflections at a higher rotation speed was attributed to the frictional force at the flap hinge. The introduction of a thrust bearing was found to dramatically improve flap performance at higher rotational speeds (±5 deg at 800 RPM in the vacuum chamber and ±2 deg at 750 RPM on the hover stand). Again, on the hover stand, there was a severe degradation of flap performance at the operating speed (900 RPM).

Koratkar [49] developed an improved analytical model of the coupled bimorph-flap dynamics including time-domain unsteady aerodynamics (Hariharan-Leishman [50]), and centrifugal, inertial and frictional forces. The linkage arm length associated with mechanical amplification mechanism was selected in order to maximize flap performance in the rotating environment. Through systematic testing of a 2-bladed rotor model in the vacuum chamber, the slippage of the bimorph under high centrifugal loads was discovered to be the culprit for performance degradation at high rotational speeds. An improved clamping of bimorph actuator (Fig. 3) showed a dramatic improvement of flap performance. In hover, flap deflections of ±4 to ±8 degrees were achieved for 1/rev to 5/rev excitation at 900 RPM (Figs. 4 and 5). This flap activation resulted in a 10% variation of steady rotor thrust at a collective pitch of 6 degrees. Systematic validation of analytical model was carried out using test data from a series of bench tests, vacuum chamber tests, and hover tests. Using this analysis, a feasibility study of a Mach-scaled rotor model with piezo-bimorph actuated flaps was carried out. Also, it was shown that a higher voltage can be applied in the polarization direction than that against this direction thereby extending the peak-to-peak excitation field. This study showed that flap deflections of ±6 degrees at 4/rev excitation could be obtained at the Mach-scaled operating speed of 2150 RPM using a 8-layer tapered piezo-bimorph in conjunction with a bias voltage (unequal voltage to top and bottom sheets) (Figs. 6-8).

Subsequently, a four-blade Mach scaled rotor model of diameter 6 feet with piezoelectric bender actuated flap was built [46, 51] (Fig. 9). From analysis, it became quite clear that an 8-layered tapered actuator with a bias voltage is needed to obtain the desired actuation authority. This model was designed for Mach scaled hub of Bell-412 model. Model rotor test in the vacuum chamber showed a marked degradation of performance at 2000 RPM. A maximum flap deflection of ±3.2 degree was achieved at 95 Vrms with 3:1 AC bias at 10 Hz; less than half of the predicted value (Fig. 10). This degradation was traced to frictional force at the blade-flap interface. Subsequently, a micro-thrust bearing was specially mounted on the flap shaft to reduce this frictional force and it resulted in flap deflections of over ±8 degrees at 2000 RPM in the vacuum chamber. This model was tested on hover stand (Fig. 11) and it achieved ±6 to ±10 degree flap deflections at a RPM of 1850 and an over 10% oscillatory thrust (Fig. 12).

A 4-bladed Mach-scaled rotor model was tested in the Glenn L. Martin wind tunnel using the Bell-412 hub in both open- and closed-loop studies [52] (Fig. 13). In open-loop tests, flap deflections of ±4 to ±5 degrees were achieved at 1800 RPM over a wide range of advance ratios and collective settings. Preliminary closed loop tests conducted using a neural-network based adaptive controller demonstrated the control authority of actuation system by minimizing the 4/rev vertical hub shear by 40% with one activated flap. In another test, a large 1/rev flatwise bending moment near the blade root was actively minimized by 90%. It is planned to expand the close-loop tests in the wind tunnel.

Spnagler and Hall [53] and Prechtl and Hall [54] built wing models with piezobimorph-driven flaps respectively incorporating mechanical hinges and flexural amplification mechanisms. It was shown that the efficiency of the bimorph actuator could be improved by tapering its thickness with length, and the frictional losses at hinges and backlash could be minimized through the use of a flexural amplification mechanism. Flap deflections of 11.5 degrees were demonstrated in a non-rotating environment. Fulton and Ormiston [55] built a 7.5 ft diameter two-bladed Froude-scaled rotor model with a plane trailing-edge flap actuated with piezo-bimorphs and tested on hover stand. A maximum of ±5 deg. of flap deflection at 760 RPM was achieved. Subsequently, this rotor model was tested in the wind tunnel to investigate the effectiveness of on-blade elevon control to reduce vibratory loads [56]. The open loop tests successfully demonstrated the effectiveness of flaps to minimize 3, 4, and 5/rev blade vibratory bending moments at representative advance ratios.

Normally, plane trailing-edge flaps are integrated into the blade profile and often characterized as "lift flaps." For these, oscillatory flap generates primarily oscillatory lift on the section along with a small component of oscillatory moment. On the other hand, servo flaps are auxiliary airfoil sections, located outside of main blade profile and are often characterized as "moment flaps." It is perceived that an oscillatory motion of flap generates primarily

oscillatory moment. Koratkar [51] carried out a study to investigate the effectiveness of these two types of flaps. It was found that twist generated due to the moment action of plain trailing-edge flap was substantial (.2 deg at 1/rev to .65 at 4/rev) and hence should be included to check flap effectiveness. Fulton and Ormiston [55] showed that at a high dynamic pressure, this moment action could cause control reversal.

To build a full-scale rotor using this concept, a design study was conducted to achieve a trailing-edge flap deflection of ±4 degrees. Fig. 14 shows actuator size for three different rotor scales. This shows that it is possible to build a full-scale system using a 40-layered bimorph, but at a considerable weight penalty. Overall, the concept appears suited for scaled rotor models and especially to check the effectiveness of adaptive control strategies to minimize vibration with trailing-edge flaps.

2.2 Trailing Edge Flap Actuated with Piezo Stacks

In a piezo stack actuator, a large number of thin piezoceramic sheets are bonded together by means of conducting adhesives (Fig. 15). Voltage is applied through electrodes attached lengthwise on opposite sides of stack. The displacement of the device in the direction normal to its plane is given as:

$$\delta = n\, d_{33}\, v \qquad (1)$$

where δ is displacement, n is number of piezo sheets, V is applied voltage and d_{33} is piezoelectric constant. The value of d_{33} is positive and is normally about 2 to 3 times of the value of d_{31} (peizo constant to define strain in the plane of sheet). With an electric field, each sheet expands in the thickness direction thus causing stack elongation. Bond layer thickness between sheets reduces the effective deflection. It is important to note that for a given piezoceramic material, a higher value of transverse displacement (stroke) can be obtained by using a large number of piezoceramic sheets and by reducing the bond thickness.

Piezoceramic stack actuators are high force and low displacement devices and it is possible to trade force for displacement by mechanical means. Samak [6] explored this possibility of using piezostack actuator with mechanical leverage amplification (Fig. 16) to actuate a 'flaperon' consisting of a small movable surface hinged at 10% chord of wing model with a span and chord of 12 inch. The objective of this flaperon was to improve stall characteristics of the airfoil by energizing the flow near its leading edge. The free displacement of the chosen piezostack was 0.72 mil at 150 volts. A mechanical amplification of 25 was used. However, because of mechanical losses and slippage at knife edges, the free displacement of the device was found to be 5 mils as compared to the calculated value of 18 mils. Samak [6] also built a leading-edge droop actuation using an electrostictive stack actuator in conjunction with mechanical amplification. Again, like piezo-stack actuation, this device could not achieve the desired amplification of stroke. It was quite clear that the amplification system needed to be refined before the potential of these devices could be realized in full-scale applications.

Spencer [52] employed two piezostacks and L-arm amplification (Fig. 17) to actuate a trailing edge flap in a wing model of chord 8 inch and span 10 inch. A single plane flap of chord 1.6 inch and span 4 inch was built. Two piezostacks bonded together back to back yielded a free displacement of 1.5 mils which was amplified 10 times. The measured value of free displacement was 11 mils as against the calculated value of 15 mils. Thus the mechanical losses in this device were less dominant. The linear motion of the actuator was converted to rotary motion for flap actuation using a hinge offset mechanism. This wing model was tested in an open-jet tunnel, and the performance of the flap degraded at high dynamic pressures. No-velocity flap amplitude of ±3.5 degree was reduced to ±1.5 degree at a forward speed of 118 ft/sec. Even though the measured values of flap deflections at high dynamic pressures were less than one-half of the predicted values, this showed the room for improvement of the amplification system.

Chandra[58] improved the actuation system of the trailing-edge flap in a wing model using a high performance piezo-stack actuator with integrated mechanical amplification (flexure and no hinges, Fig. 18). The composite wing model was of 8 inch in chord and 16 inch in span (Fig. 19). Measured free displacement and block force of this actuator were respectively 28 mils and 16 lbs at 1000 volts excitation. The flap deflection was measured using a Hall effect sensor, and a maximum of 6.5 degrees of free flap deflection was achieved. As predicted, a 30% reduction of flap deflection at a free stream velocity of 95 ft/sec in an open-jet wind tunnel was noticed (Fig. 20). Angle of attack of 10 degree did not change flap deflection. To simulate the full-scale aerodynamic forces for a typical rotor blade, the performance of several commercially available actuators was examined for flap actuation. The calculated results show the feasibility of a full-scale flap actuated with a piezo-stack actuator to minimize vibration (Fig. 21).

Lee [9,59] carried out systematic testing of eleven different piezostack actuators to evaluate their characteristics that include maximum free strain, maximum block force, elastic modulus, operating voltage and shape/compactness. Tests were carried out first with static excitation and preload (0-10 ksi) and then followed by dynamic excitation. Because the piezostacks were different in shape and size, a strain-force index consisting of a product of free strain and normalized block force as well as an

energy density index were used for comparison. Based on these indexes, two actuators respectively built by two different companies showed superior static performance (Table 1). Further dynamic tests showed that the first category of stacks resulted in constant actuation envelope for all ranges of preloads while the second category stacks tended to increase envelope with preloads. The first category stacks with higher stiffness as well as dynamic characteristics were selected. Using five of these stack actuators, a double-lever (L-L) amplification device was built to actuate a full-scale trailing-edge flap (Fig. 23) [59-60]. The design goal was to obtain flap deflection of $\pm 5^{o}$ at the nominal speed for the Boeing MD-900 Explorer helicopter. A model wing section of chord 12" and span 12" and with a flap of span of 4" and chord 3" was built (Fig. 24). The first prototype of the amplification device was tested in the vacuum chamber and an amplification factor of about 19 was achieved for a 600g of centrifugal loading. Further design refinements were introduced to build the second version of this actuator that achieved a peak actuation force of 18 lbs and a stroke of 43 mils for a 710g of centrifugal loading in the vacuum chamber (Fig. 25). For the spin test, a coil spring was mounted at the outer lever to simulate aerodynamic loading. At 1000 RPM, no major degradation in peak-to-peak output displacement was observed for up to 6/rev excitation. Subsequently, this model was tested systematically in the open-jet wind tunnel to check its performance under different aerodynamic loading. The flap was actuated using a push rod arrangement and it achieved peak-to-peak flap deflections of 4 to 20 deg. depending on excitation frequency at a speed of 120 ft/sec (Fig. 26) [61]. One drawback of this actuator was its single directional actuation. Restoring spring was used to make it bi-directional, but it degraded at high dynamic forces. As a result of it, a bi-directional actuator with L-L amplification mechanism is being built. This concept consists of two unidirectional L-L amplification mechanisms in a parallel arrangement that can offer high force and high displacement capability without compromising its compactness.

Straub et al [62-65] are developing a stack-actuated trailing-edge flap for the MD-900 Explorer rotor system (5-bladed, 34 ft bearingless rotor) to actively control its vibration, noise and aerodynamic performance. Based on the energy output (stroke and force) for a prescribed volume, the piezo-ceramic/lead magnesium niobate stack was initially selected (low-voltage, co-fired PMN:PZ stack developed by Xinetics). The required large deflection is accomplished using a bi-axial arrangement of two long stack columns operating in push-pull mode in conjunction with L-shaped lever and flexural mount [Fig. 27]. The flap length is 18% radius and it is centered at the 87% radial position. A detailed design was carried out to meet the severe operating environment (665g steady load, 90g oscillatory, -60 to 160^{o}F). The flap was expected to undergo ± 4 deg at 40 Hz with an actuation force of 112 lbs. The stack actuator however did not realize the projected potential. Flap sizing and aerodynamic optimization to minimize actuation power were discussed in Ref [64]. Recently, a series of enhancements were made to the design of the actuation system including high energy density piezostacks [65]. The performance of this bi-axial actuator was demonstrated through testing in a spin chamber under 814g steady and 29g vibratory loading. Selected configuration consisted of a 25% flap chord, a span of 18% radius and an aerodynamic balance of 40%. Prechtl and Hall [66] designed a discrete trailing edge servo-flap actuator called X-frame actuator [Fig. 28] and tested the prototype (150% of model scale) on the bench top test. The actuator consists of two active piezostacks and two criss-cross frames and amplification is achieved via shallow angle arrangement. The X-frame achieves a higher mass efficiency but requires larger frame dimensions than that of lever amplification mechanism. A 1/6th Mach scale rotor model of CH-47D (Chinook) incorporating a trailing-edge flap actuated by X-frame actuators was built and tested on a hover stand [66]. This flap extends aft of the main blade chord. At the operating speed (tip Mach .63) and collective pitch of 8 deg., oscillatory flap deflections of ±2.4 deg. were achieved with an excitation of ±1 KV. The X-frame actuator has been selected for the MD900 Explorer active flap of a full-scale system. To obtain bi-directional functionality, dual X-frame actuators are being built. The proposed flap has 18% span, 25% chord and 40% hinge offset and is located at 83% radial position. The full-scale rotor system with trailing-edge flap actuated with X-frame actuators is under fabrication and is planned for testing on the whirl tower, followed by testing in the 40x80 ft wind tunnel at NASA Ames and finally by flight testing. Janker and et al [36, 68-69] developed a piezostack-based actuator for trailing-edge flap. Amplification device consists of a shallow angle flexure mechanism that is wrapped around the stacks. The performance of this actuator was demonstrated through testing of wing-section in the wind tunnel. It is estimated that an actuator with block force of 2000 N and free displacement of 1mm will be adequate to achieve a target flap deflection of ±8 deg. for an EC-135 helicopter. It planned to investigate this actuator on a rotor model in the wind tunnel.

Shaner [37, 70] carried out design and development of piezostacks-actuated leading-edge flap. Stroke amplification was achieved through a single lever. Bench-top tests were performed to evaluate its performance. Even though the current prototype did not achieve the desired stroke output, potential problems were identified and future testing of wing section in the wind tunnel is planned. Janker and et al [36] also examining peizostack-based

actuator for leading-edge droop control for delaying dynamic stall.

Overall, the actuation of flaps with piezostacks appears feasible for full-scale applications. Even though it may not be cost effective to apply this actuation mechanism to minimize vibration and exterior noise with currently available smart materials technology, but there is an enormous potential with future large stroke actuators.

2.3 Trailing Edge Flap Actuated with Magnetostrictive Actuators and Extension-Torsion Coupled Composite Tube

For a full-scale trailing edge flap system, the force requirement of actuators becomes substantial. At the same time, the blade can also accommodate larger size actuators. An alternate concept of using extension-torsion coupled composite tube in conjunction with magnetostrictive actuator was investigated to cause twisting of the trailing edge flap [7]. Figure 29 shows a schematic of this concept. The extension-torsion composite coupled tube was subjected to an axial force generated by a magnetostrictive actuator that induces twisting of the tube. An extension-torsion composite beam was built by wrapping angle plies resulting in an anti-symmetric ply lay-up with respect to the beam axis.

A thin-walled beam analysis developed in Ref. [71] was specialized to predict the induced twist of an extension-torsion coupled composite cylindrical tube due to axial force. The essence of this analysis is that two-dimensional stress and displacement fields associated with any local plate segment of the tube are reduced to the global one-dimensional beam displacements and forces (Vlasov theory). Non-classical effects such as cross-section warping, transverse shear and warping restraint at edges were included. The objective was to determine the design of the composite tube that best utilizes the prescribed force and displacement characteristics of the magnetostrictive actuator to generate maximum torsional motion. To understand the influence of ply lay-up, number of plies and tube diameter on the induced twist, extensive parametric studies were carried out. Three different composite materials, graphite-epoxy, kevlar-epoxy, and glass-epoxy were examined. Figure 30 shows that for a prescribed axial force, the maximum induced twist occurs for kevlar-epoxy tube with a ply angle of approximately 30 deg. Then an optimization study was carried out to calculate the best tube design keeping in view first ply failure and buckling instability.

The magnetostrictive actuator was selected because of its large actuation force as compared to electrostrictive and piezoelectric stacks. For the present study, a commercial available magnetostrictive actuator (100/6-MP Etrema) was chosen. In order to utilize the extension-torsion coupling characteristics of the composite tube, the magnetostrictive actuator must be attached to the tube in such a way that both twist and axial strain is permitted freely. Figure 31 shows the schematic of the tube and actuator assembly. A series of tests were performed to check the performance of this torsional actuation device for different loading.

To validate the analysis, extension-twist kevlar-epoxy tubes of different ply lay-ups were fabricated using an autoclave molding technique. These tubes were first tested under static mechanical loads and then tested under manetostrictive actuation. Tip twist was measured using a laser optical system. The $[11]_2$ tube generated the maximum twist of 0.2 degree and there was a good correlation between measured and predicted twist values (Fig. 32). Also, alternate actuator concepts for these tubes, specifically piezoelectric and electrostrictive stacks, were examined. A piezoelectric stack was found to induce much larger force and twist (approximately 3 times that created by magnetostrictive actuator system). It was shown that ten $[11]_4$ kevlar-epoxy tube/piezoelectric stack systems of 20 inch length in series would generate approximately ±5.2 degrees of flap deflection. Such a system can be implemented in a full-scale rotor to actively control vibration.

Because of poor overall structural efficiency of extension-twist coupled tubes, this type of actuation system appears less meritorious than other actuation systems.

2.4 Trailing Edge Flaps Actuated with Piezoceramic Actuators and Tailored Bending-Torsion Coupled Composite Beam

This section presents the development of a dynamically scaled rotor model with torsional actuation via a piezo-induced bending-torsion coupled composite. A novel spanwise variation in ply lay-up of the beam and phasing of surface-mounted piezoceramic actuators is used to convert the bending-torsion coupled beam into a pure twist actuator [72-76]. This twist actuator is used to actuate either a trailing edge flap (Fig. 33) or an all-movable blade tip or induced blade twist (Fig. 34). The beam is divided into a number of spanwise segments with reversed bending-torsion couplings for each successive segment. Over each beam segment, identical piezoceramic actuators are bonded on the top and bottom surfaces resulting in an equivalent bimorph unit (Fig. 35). Again, the polarity is reversed for successive piezo elements. This composite beam is located spanwise within the blade profile at about quarter-chord. The beam is clamped in an anchor at the root of the blade and has a radial bearing at the outboard end. An excitation generates a sinusoidal spanwise bending where as the induced twist is additive in the spanwise direction (Fig. 36).

For the trailing edge flap configuration, the flap is an integral element of the outboard end of the

beam (Fig. 33). As the tip of the beam twists relative to the root end (cantilevered), the flap rotates too. For movable tip configuration, the blade tip segment is attached to the outboard end of the beam via a rigid adapter and a radial bearing (Fig. 34). As the tip of the beam twists, the blade tip is torsionally deflected. For the induced blade twist configuration, the outboard end of the beam is locked to the end-rib of the blade. Thus, as the tip of the composite beam twists, it will induce twist in the entire blade.

A two-bladed rotor model (dia 6ft) was tested on the hover stand using a bearingless rotor rig to evaluate the performance of this actuation system at various rotational speeds and collective settings. The actuation mechanism was excited at various frequencies and RMS voltages. First, the trailing-edge flap concept (span 3% radius and chord 20%) located at 90% radial position was tested systematically. In Fig. 37, the flap deflection is plotted vs. rotor speed for different excitation voltages. The excitation frequency is set at 40 Hz and collective is zero. As shown, the flap deflection does not decrease with rotational speed. Because of a large actuation force, the flap deflection stays constant with rotational speed. It was also shown that the effect of collective setting on flap deflection was negligible. The peak-to-peak flap deflection of 4 degrees was obtained at the operating speed of 900 RPM. From the results, it is quite clear that a larger flap can be driven with this bending-torsion device.

To follow on, two movable-tip rotor models respectively with 5% and 10% tip span were manufactured and tested systematically in a two-bladed configuration. Initially, the controllable twist configuration was tested on the hover stand at various excitation frequencies and collective settings. A non-rotating blade tip amplitude of .65 degree at 75 Hz was reduced to .5 degree at a RPM of 875 (Fig. 38). Then, hover testing was carried out on movable-tip configurations. At a RPM of 875 and a collective pitch of 8 degree, oscillatory tip pitch amplitudes of about ±2 degree were obtained at 2, 3, 4, 5/rev excitation with a corresponding dynamic thrust of about 7.5% of steady value [73]. Subsequently, a coupled actuator and elastic blade aeroelastic analysis was developed to predict the performance of an active-tip rotor [74]. The hover test data obtained from the Froude-scale rotor model were used to validate analysis. Predictions of active blade pitch deflections and vertical root shear were within 20% of measured values.

Subsequently, a 4-bladed Mach-scale rotor model with 10% tip was built for testing at an RPM of about 2000 in hover using Bell 412 hub [75, 76] (Fig. 39). For an actuation of 125 V_{rms}, the measured blade tip deflection at the first four harmonics was between ±1.2 and ±1.6 deg (Fig. 40). At 2000 RPM and 5/rev excitation, a large tip response is due to resonance amplification. Again, there was no degradation of tip response with rotor speed and aerodynamic thrust authority was in the range of 10% to 30%. The performance of blade tip deteriorated at high collective pitch because of locking of shaft in the bearing. Redesign of blade tip shaft assembly was suggested for future improvement of this concept. In a parallel study, active tip rotor was re-configured to test it in an active twist mode. The blade tips were taped down to prevent relative twisting between the tip and main blade section and actuation of beam resulted in twisting of complete blade. Even though the rotor was not designed for active twist mode, a significant tip twist was observed; 0.78 deg in non-rotating condition to 0.83 deg at 2000 RPM. Closed-loop tests were conducted using a neural-network based adaptive controller to minimize background vibratory blade loads [76]. The algorithm used a combined Kalman filter and a single hidden layer neural network to learn the system dynamics and minimize the desired vibration objective function online in real time. A large 1/rev vertical hub load as a result of blade dissimilarity was minimized by 90% using this controller. In another test, the controller was asked to minimize the simulated vibratory root flap bending and rotor thrust (target amplitudes) and it successfully minimized these by 80 to 95%.

Analyses and tests so far have demonstrated the feasibility of such a solid state torsional actuation device for active control of vibration and acoustics. It will be important to develop a comprehensive coupled rotor analysis including modeling smart actuator, validate it with measured test data and then carry out parametric studies to investigate the potential of this concept for a full-scale system. This innovative concept shows potential for control of vibration and noise for a full-scale system especially as a partial reduction auxiliary device.

3. Controllable Twist Blade with Embedded Piezoceramic Actuators

This section presents the development of a dynamically scaled rotor model where blade twist is controlled using distributed embedded piezoceramic actuators [77-81]. Specially-cut piezoelectric actuators are attached under the skin at an orientation so that a pure twisting of blade occurs when the same potential is applied to both top and bottom actuators.

The smart rotor model was built with a six-foot diameter, 1/8-th Froude scale, four-bladed bearingless rotor (Boeing-ITR). The blade was constructed by laminating 10 mil pre-preg fiberglass cloth plies around a foam core, which was cured in a NACA 0012 airfoil mold (Fig. 41). The overall blade length was 26.58 inches from tip to root and the chord was 3.0 inches.

Structural integrity was achieved through a mahogany wood root section and a continuous longitudinal 10 mil fiberglass spar with ply angles of

[0/90] degrees, which was embedded at the quarter chord location. Bringing the airfoil section center of gravity at quarter-chord by placing tantalum weights near the leading edge reduced inertial coupling between the flap and pitch modes. To activate blade motion independently in bending and torsion and to sense blade deformations, specially shaped 11.5 mil thick for single-layer piezoceramic actuators, and 23 mil for dual-layer actuators, were embedded under the fiberglass skin in banks of five discrete elements at angles of ±45 degree respectively on the top and bottom surfaces of the blade. Wires extend from each bank to the root of the blade, allowing for independent actuation of each bank. The piezoceramic actuators (PZT-5H, Morgan-Matroc) used for this study were cut to dimensions of 2.0 inches in length and 0.25 inch in width to minimize transverse actuation. The dual-layer actuators were manufactured by bonding two single-layer actuators using a high temperature cyanoacrylate (CA) adhesive. Total number of actuators per blade range from 24 (single-layer, 1.5 inch apart) to 120 (dual-layer, .75 inch apart). A twist distribution along the blade span was achieved through an in-phase excitation of the top and bottom actuators at equal potentials, while a pure bending distribution is achieved through an out-of-phase excitation.

The structural properties of the piezoceramic blade were experimentally determined by measuring the spanwise bending and twist distributions along the blade. A laser beam was reflected off mirrors mounted at the elastic axis along the span of the blade and several tip loading were used to determine average values for the structural stiffness. The measured flapwise and chordwise bending stiffness were within 25% of target values, whereas the measured torsional stiffness was over 40% of the desired Froude-scale value for some blade configurations. Keeping in view the complexity of the fabrication process, the overall range of variation of stiffness was within an acceptable level. Generally, a close spacing of actuators increased the stiffness.

To assess the effect of bond thickness on actuator performance, simple blade specimens were built and tested under a static field [79]. The bond thickness was varied from 0.0025 inch (close to perfect bond condition) to 0.02 inch (not too abnormal) and the orientation of actuators was varied from 0º (aligned with beam axis) to 65º. Also, uniform strain beam theory for embedded skewed actuators including effect of bond layer was developed and compared with test data. The effect of reducing the bond thickness can be seen in Fig. 42. The maximal torsional and bending deflections increased by 60 and 90% respectively when the bond thickness was reduced from 0.020 to 0.0025 inch. A minimal bond layer thickness results in the most efficient shear transfer, which in turn results in maximum torsional and bending response. An optimum blade twist actuation will result for perfectly bonded actuators oriented at skew angles of ±45 degrees.

The effect of spacing between actuators was investigated by a series of blade test specimens with spacing ranging from 0.1 inch to 2.0 inch [79]. Test results showed that increasing the actuator spacing reduced the structural stiffness of the blades, as well as the nonlinear interference effects. A simple block force beam model was formulated for two overlapping skewed actuators and satisfactorily validated with test data. The nonlinear interference effect was observed to have reduced the twist by up to 38% when the spacing was reduced from 1.5 to 0.1 inch. If the overlapping between two adjacent actuators is reduced to zero, the interference effect is non-existent.

To assess the effectiveness of the embedded actuators in the rotating environment, the blades were tested first, in a two-bladed bearingless rotor configuration on a hover tower, and later on as a four-bladed configuration in the Glenn L. Martin wind tunnel [80]. Single and dual-layer rotor configurations were tested for varying electric field for different excitation frequency and tip twist was measured using two micro-accelerometers placed at the blade tip. Tip twist of the order of .4 degree at 4/rev was obtained in both hover and forward flight (μ=0.33) (Figs. 43). The change in oscillatory thrust, torque, pitching moment and rolling moment were measured using a rotating frame balance (Fig. 44). A maximum increase in oscillatory rotor thrust, torque, pitching moment and rolling moment (as percentage of nominal steady-state values) of 11, 13, 6 and 10%, respectively was measured for the dual-actuator configuration.

Although the oscillatory twist amplitudes attained in the forward flight experiments were less than the target value (1-2 degree of tip twist for complete vibration suppression), it showed the potential for partial vibration suppression. A feasibility study was carried out to apply this methodology on a typical full-scale rotor system (UH-60) to minimize vibration. Using today's commercially-available actuators, it is possible to build a full-scale controllable-twist blade with embedded multi-layered piezoceramic actuators that can completely suppress vibration, but at a considerable weight penalty (16% of blade weight) [81]. However, this scheme of actuation shows potential for a partial active control of vibration and acoustics.

Hagood et al [82-85] built a controllable-twist blade by embedding distributed piezoelectric fibers in a composite blade (Fig. 45). By laying piezo fibers at ±45º to the blade axis, and actuating the piezo material along the fiber direction using an interdigitated electrode pattern, it induces blade twist. The actuation of the active fiber composites induces shear stresses in the spar, resulting in a linear twist along the length of the spar. Using this

active fiber composite (AFC), a 1/6th Mach-scaled rotor model of the Chinook CH-47D was constructed with a weight penalty of 20% of blade weight to cause a ±2º of blade tip twist. A high excitation voltage of 1.7 KV is needed to achieve desired twist. The model was tested on their hover stand and a maximum of tip twist of .4º was achieved [85]. Low tip twist was attributed to actuator electrical failures and manufacturing defects. However, it demonstrated the feasibility of this concept for a Mach scale rotor system. Again, this technology shows potential for full-scale applications provided compact high-voltage slipring is developed and structural integrity of a blade with fibers is improved.

4. Shape Memory Alloy Actuators

Shape memory alloys (SMA) such as Nitinols can undergo large plastic deformation via extension, bending or twisting at room temperature and then recover the deformation (i.e., recover to original shape) upon heat activation. Large strains, on the order of 6% can be recovered with a moderate increase in temperature (say to 120ºF). Mechanically restrained SMA wires can develop large tensile recovery force due to the shape memory effect. Also, there is a dramatic increase in modulus of elasticity of SMA at a high temperature. These characteristics can be exploited in different applications. Even though SMA actuators can result in high strains and high forces, frequency range is very small (less than 1 Hz) that restricts these actuators to mostly static applications.

There are four transition temperatures associated with SMA materials [4]. These are martensite start, M_s, martensite finish, M_f, austenite start, A_s, and austenite finish, A_f temperatures. In the heating cycle, for temperature below A_s, the material is in the 100% martensite phase, where as for temperatures above A_f, the material is in 100% austenite phase. In the cooling cycle, for temperatures above M_s, the material is in 100% austenite phase, where as for temperature below M_f, the material is in 100% martensite phase. At any other temperature, the SMA's is in mixed phase, partly matensite and partly austenite. The state of SMA is characterized by the volume fraction of the martensite phase ξ that depends on temperature, stress and initial state of material.

Using shape memory effects, there is the potential of designing a variable speed rotor, trailing-edge tab adjustment for in-flight tracking of the main rotor, supercritical tail-rotor shaft and collective pitch control system (without swashplate). To accomplish these goals, understanding of constitutive models of SMA and development of analysis and fabrication of thin-walled composite beams with embedded SMA wires is important.

Even though several constitutive models of SMA are developed to characterize its thermo-mechanical behavior, these are not validated systematically for different load conditions. These models are based on thermomechanics, or a combination of thermo-mechanics and SMA phenomenology, and/or statistical mechanics. One of the earliest models was developed by Tanake [86] that is based on thermo-mechanics. In this model, the second law of thermodynamics is written in terms of the Helmholtz free energy. This model assumes that stress (σ), strain (ε), temperature (T) and the martensite volume fraction (ξ) are the only state variables needed to characterize shape memory alloys. The stress consists of three parts, the mechanical stress, the thermoelastic stress, and the stress due to phase transformation. The constitution equation is as follows:

$$(\sigma - \sigma_o) = E(\xi)(\varepsilon - \varepsilon_o) + \Theta(T - T_o) + \Omega(\xi)(\xi - \xi_o) \quad (2)$$

where subscript 'o' represents the initial condition of SMA. Note that the Young's modulus (E) and the phase transformation coefficient (Ω) are function of the martensite volume fraction. Tanake used an exponential expression to describe the martensite volume fraction in terms of temperature and stress. Liang and Rogers [87] developed a constitutive model similar to Tanaka's model, except that they used a cosine function to represent the matensite volume fraction. Brinson [88] modified these two models by dividing the matensite volume fraction into two parts, stress-induced martensite and temperature-induced martensite. Also, the coefficients of the constitutive model are assumed to be non-linear and are resolved about the initial matensite state. Boyd and Lagoudas [89] utilized the Gibbs free energy instead of the Helmholtz free energy to obtain the constitutive model. The martensite volume fraction is derived from the dissipation potential, and by satisfying the second law of thermodynamics.

The stress-strain curve for an SMA consists of three regions: (1) elastic region where no transformation occurs, (2) transformation region where stress-induced matensite forms, and (3) yield region where permanent deformations occur (Fig. 46). The material constitutive models vary considerably in three regions. So far, only a few limited validation studies have been carried out to evaluate these constitutive models. Epps [4] carried out systematic testing of a 20 mil Nitinol wire to obtain its thermo-mechanical characteristics including stress-strain (fixed temperature) and strain-temperature (fixed stress) curves, and then evaluated above four constitutive models using these test data. Figures 47 shows the measured and calculated stress-strain curves at 100ºF and 140ºF respectively representing mixed mode (both martensite and austenite phases exist) and austenite phases. It was

concluded that all models correlate well with test data as long as the constants for the constitutive models are derived properly from the test data. Especially the model developed by Brinson showed a clear distinction between temperature-induced and stress-induced matensite volume fractions. Prahlad [5] carried out a systematic quasistatic testing of NiTi wire at constant temperature, constant stress and constant strain to determine the extent of variation of properties depending on the path of testing. It was pointed out that the state of material is not unique at points along the transformation, and is a function on not only the state variables but also the history, path of loading, strain rates, loading pattern and boundary condition. This behavior is likely to be critical to the application of SMA in devices involving dynamic loading.

Rogers, Liang and Jia [90-91] analytically studied the behavior of shape memory alloy reinforced composite plates. They demonstrated the structural control characteristics and authority with the SMA reinforcement for four different plate problems; plate bending, free vibration, buckling analysis, and acoustic transmission loss through the plate. It was shown that the first bending frequency of a simply supported composite plate increased by about 100% at activation for 10% SMA reinforcement (by volume). Rogers and Barker [92] presented an experimental study of active strain energy tuning of composite beams with embedded SMA. The beam and the SMA wires were independently clamped. They showed the fundamental bending frequency of a clamped-clamped graphite/epoxy beam increased by about 200% with 15% nitinol volume fraction. These early studies showed the potential of controlling static and dynamic characteristics of beams and plates using embedded SMA fibers. However, no correlation of test results with predictions was made. Baz, Imam and McCoy [93] conducted a study on the active vibration control of flexible beams with SMA wires mechanically constrained on the exterior of the beam. The recovery force due to heat activation was used to change the dynamic characteristics of the beam. In another study, Baz et al [94] inserted SMA wires into a flexible beam with sleeves to control its buckling and vibration behavior. SMA wires were clamped separately. They showed that the buckling load of fiberglass composite beam could be increased three fold upon heat activation. Epps and Chandra[95] embedded SMA wires with sleeves into solid graphite-epoxy composite beam and showed a 22% increase in the first bending natural frequency with a 2% nitinol volume fraction (Fig. 48). Vibration analysis of a composite beam with SMA wires was developed by assuming separately constrained SMA wires as an elastic foundation for the main beam. The spring constant of elastic foundation depends on the recovery force in the SMA wires. Finite element analysis showed good correlation of fundamental frequency with test data for different temperatures. A numerical study by Epps and Chandra[96] showed that embedded SMA wires with sleeves can be used for active tuning of composite shafts. For example, 25 SMA wires of 20 mil diameter embedded into a graphite-epoxy beam of 30 inch length, 1 inch width and 62 mil thickness increase its first bending frequency by 276% on heat activation.

There are two important considerations for embedding SMA fibers in composite beam [96]. The first one is that the matrix of composite material should withstand the prestrain of the SMA fibers. This requirement does not permit the use of normal composite materials and calls for the use of materials with superior interlaminar shear strain at failure. IM7-8552 from Hercules appears to show the potential of satisfying this requirement. The second consideration is that the SMA fibers must be constrained during the manufacturing, so that these do not return to their original position at curing temperatures which are higher than the phase transformation temperature of the SMA. In order to avoid this problem of curing at high temperature, three approaches have been followed. In the first approach, composite solid beams with SMA wires were built using room temperature curing adhesive with glass-epoxy sheets. This does not need the device to constrain the SMA fibers as the phase transformation temperature of SMA (158ºF) is above the curing temperature (70ºF) of the adhesive. In the second approach, graphite-epoxy beams with fused silica tubes filled with 'dummy' steel wires were fabricated using an autoclave molding technique. In order to assure a good bond between the tubes and the graphite-epoxy material, a film adhesive was used. After curing the composite beam, the steel wires were replaced with pre-strained SMA wires. In the third approach, each one of the pre-strained SMA wires is held fixed between two ends during the curing process. After the curing cycle completed, the end restraints were released.

Currently, research activities are growing towards application of SMA to aerospace systems. One potential application is to adjust trailing-edge trim-tab of a helicopter rotor for in-flight tracking. Liang et al [97] investigated the usage of pre-twisted SMA rod to torsionally deflect the blade tab. Two concepts were examined respectively using one-way and two-way memory actuators. In the first concept, one SMA rod was used as actuator while second one as a restoring spring (differential bias). In the second concept, one SMA rod in conjunction with locking arrangement is used. Kudva and et al [25-26] examined the induced wing twist and camber control using SMA actuators in a Mach-scaled fixed-wing model. Tests of this wing model in the Transonic Dynamics wind tunnel at Langley showed potential of this device for aeroelatic control of aircraft. Hanagud and Roglin [35] demonstrated the collective control in a flying-model rotor using SMA actuators.

A study [98] was undertaken to develop a SMA-actuated trailing-edge tab (length 4% radius) for the MD-900 rotor system (5-bladed bearingless rotor) for in-flight blade tracking. This tab was located at 72% radial position and was expected to be driven by a SMA torsional actuator (developed by Memry). A locking mechanism was developed to keep the tab in position without power to the actuator. It was designed to undergo ±7.5 deg in steps of 0.25 deg. Maximum torsional actuation moments expected were 5 in-lb during forward flight and 9 in-lb during maneuvers. It was proposed to test this full-scale rotor on the whirl tower, followed by testing in the wind tunnel and flight testing.

Epps [99-102] built a wing model of span and chord of 1 foot with a trailing-edge tab of span 4 inch and chord 2.4 inch to investigate the concept of in-flight tracking of rotor blades using shape memory alloy actuators (Fig. 49). 2 to 5 nitinol wires of diameter 0.015 inch with an initial prestrain of about 3% were clamped at one side to the spar located at quarter-chord and at other side to the hinge tube attached to the tab, respectively on its top and bottom surfaces (Fig. 50). To deflect the tab downward, the bottom wires are heated (using internal resistance) while the top wires remain at room temperature. To deflect the tab back to its original position or upward, the upper wires are heat-activated, while the lower set remains at room temperature. To lock the tab at a desired angle (in power-off condition), a gear-locking mechanism consisting of spur gears, pulling solenoid, restoring spring and pawl was built. A displacement feedback controller was developed to fine tune the tab deflection in about 10 seconds. This wing section was tested in the open-jet wind tunnel and tab deflections of the order of 20 degrees were obtained at a speed of 120 ft/sec (Fig. 51). This concept appears to show the potential for further full-scale development.

5. Modeling of Blades with Smart Actuators

To fully exploit the application of smart structures technology in the rotor system, it is necessary to develop analytical tools to model blades with induced strain actuation. Two types of analytical models are needed respectively to represent controllable twist blades and trailing-edge flap blades. For both type of rotors, simple constitutive relations of smart actuators under different loadings are required. For the comprehensive aeroelastic analysis of a rotor system, it becomes essential to treat the blade as one-dimensional beam undergoing extension, bending and torsion deformation. For such an analysis, key elements are: modeling of a beam with surface-mounted or embedded actuators, modeling of actuators with axial force and restraint, unsteady aerodynamics especially pertaining to flaps, and integration of dynamics into rotor analysis.

Crawley and de Luis [42] formulated a uniform strain bending model of a beam with strain-induced piezo-actuation. A pair of piezoceramic actuators aligned along the beam axis was assumed, and the shear lag effects of the adhesive layer between the piezoceramic actuators and the beam were included. Predicted response of the first two bending modes of a cantilevered beam was verified experimentally. Crawley and Anderson [43] formulated a Bernoulli-Euler model and compared it with uniform strain model, detailed finite element model and experiment. It was shown that for thin beams, Bernoulli-Euler model is more accurate than uniform strain model. Chandra and Chopra [103] developed a formulation for coupled composite thin-walled beams with distributed actuators and then validated analysis with experimental data. Analysis was based on Vlasov theory where two-dimensional stress and displacement fields associated with any local plate segment of the beam are condensed to one-dimensional generalized forces and moments. Correlation with experimental data from a cantilevered graphite-epoxy beam with surface mounted piezoelectric actuators (Fig. 52) showed that the inclusion of chordwise bending is essential to accurately predict a beam's coupled response (Fig. 53).

These analytical models [42, 43, 103] are developed for a pair of piezoceramic actuators, one on each surface aligned along the beam axis. If the same voltage is applied to both piezoceramics, it will result in pure extension for an isotropic beam, and if opposite voltage is applied it will result in pure bending. If the piezoceramic actuator is attached at an arbitrary orientation with respect to the beam axis, it will cause extension, bending and torsional deformation. Park et al [44-45] formulated one-dimensional analytical model of a beam actuated by single piezoceramic actuators surface-mounted at an arbitrary orientation with respect to the beam axis (Fig. 54). Both uniform strain and Bernoulli-Euler models were developed and shear lag effects due to a finite thickness of adhesive layer between the piezoceramic and beam were included. The actuator was assumed to be a line element and only permitted to induce strain in its lengthwise direction. Analysis is also applicable to distributed actuators on both top and bottom surfaces. Experimental tests on response of cantilevered beams with piezoceramic actuators were carried out to evaluate the accuracy and limitations of the models. The bending and coupled bending and extension models showed acceptable correlation with static test results whereas the combined extension, bending and torsion model showed poor correlation especially at high actuator orientation angles. Consequently, the coupled model was modified to include effects of section warping. It improved prediction of torsional response somewhat, but it is still not satisfactory for larger orientation

angle of actuator with respect to beam axis (Fig. 55). Detailed strain measurements indicated that transverse actuation is not negligible for all actuator orientations and needs to be included to refine the analysis. Modeling of a beam with

Recently, there have been several efforts to develop comprehensive aeroelastic analyses for rotors with trailing-edge flaps. Current analyses however assume prescribed flap deflections and hence neglect the dynamics of actuators. Milgram [104, 105], for example, developed a comprehensive finite element rotor analysis for plain trailing-edge flaps including indicial-based flap unsteady aerodynamics [106] and a pseudo-implicit free wake model [107]. Extensive validation studies were conducted by comparing vibratory hub loads with experimental wind tunnel data (MDHC Active Flap Rotor test in TDT wind tunnel) and predictions from another comprehensive analysis (modified CAMRAD-JA). Correlations were generally fair and showed room for improvement. Subsequently, parametric studies were conducted on a four-bladed Sikorsky S-76 rotor to examine the effect of flap size, flap location and controller on the minimization of vibratory loads [108, 109]. It was shown that a small size flap (length about 10% radius and chord about 20%) located around 75% radial position requires least actuation power. Milot and Friedmann [110, 111] developed a comprehensive aeroelastic analysis for a rotor with servo-flaps and carried out extensive parametric studies that include flap sizing and placement, actuation power and blade torsional stiffness. The flap location was determined to be an important design parameter. Myrtle and Friedman [112, 113] modified their rotor analysis with an improved unsteady aerodynamic model for airfoil/flap based on a rational function approximation approach. Straub and Hasan [114] modified the comprehensive rotorcraft code CAMRAD/JA to account for account for flapped rotor and carried out conceptual sizing and design of trailing edge flaps for an active vibration control for the MD-900 helicopter. The selected flap configuration consists of a chord ratio (flap chord/blade chord) of 25%, length of 18% radius and an aerodynamic balance of 40%.

For an accurate prediction of the behavior of rotor blades with smart material acutators, it is important to include the dynamics of actuators into rotor analyses. Recently, Koratkar [46] formulated a coupled actuator-flap-rotor model in hover. This finite element linear analysis includes piezoelectric bender actuator, blade undergoing flapwise bending and torsion, and plane trailing-edge flap. Vibratory blade response due to oscillatory field showed that the effect of coupling due to trailing-edge flap dynamics is about 10% on flap amplitude. Straub and Charles [115] carried out coupled blade/flap/actuator dynamic analysis of a bearingless rotor using a multi-body, high fidelity comprehensive code CAMRAD II. Predicted results were correlated with MDART test data as well as with CAMRAD/JA results. It was shown that simplified efficient analyses (such as CAMRAD/JA) neglecting actuator dynamics are adequate to predict rotor response, conduct concept development studies and formulate control algorithms, where as detailed coupled analyses (such CAMRAD II) including actuator dynamics are necessary for prediction of blade loads and system stability. Shen [116] developed a coupled blade/flap/actuator analysis including flap and actuator dynamics and predicted results for a bearingless rotor were correlated with test data as well as with predictions from other comprehensive codes. Inclusion of actuator dynamics resulted in larger flap control angles (10% increase) as well as more actuation power (30% increase). This study showed that the coupling effect of actuator dynamics is important for the evaluation of the performance of flap, especially for a torsionally soft actuator.

Conclusions

This paper reviewed developments in smart structures technology for application to rotor systems. Two types of scaled rotors are under development: trailing-edge flap models actuated by piezoceramic or magnetostrictive actuators, and controllable twist models incorporating specially-shaped piezoceramic elements or fibers. These models were tested in a vacuum chamber, on a hover stand and in a wind tunnel to examine their potential to minimize. For both types of rotor models, the performance of the system degraded dramatically at higher rotational speeds because of higher dynamic pressure, centrifugal field and frictional moments. Shape memory alloys actuators can undergo large strokes at a very low frequency (less than 1 Hz) and are being envisaged for several applications that include in-flight rotor tracking and variable speed rotors. Analytical tools to model a smart rotor undergoing bending, extension and torsion are under development. The following conclusions are drawn:

1. Trailing-Edge Flap Actuated with Piezo Bimorphs: For a Froude-scaled rotor model in hover, a flap actuated by a piezo-bimorph was able to deflect about ±6 deg at 4/rev at the operating speed of 900 RPM. To achieve the target flap deflection of ±6 deg for a Mach-scaled rotor model (2000 RPM), an 8-layered tapered bimorph was incorporated. This model was tested in both open and closed loop studies and successfully achieved the desired flap authority at several flight conditions. Overall, this actuation system is compact and appears suited for scaled rotor models, especially to check effectiveness of adaptive control strategies. For full-scale applications, it becomes necessary to build multi-layered actuators (say 40 layers), and more importantly to develop a refined frictionless amplification system.

2. Trailing-Edge Flap Actuated with Piezo Stacks: A multi-piezostacks actuated flap in a fixed-wing model achieved ±5 to ±10 degree depending on excitation frequency at a free stream velocity of 120 ft/sec. Also, it was tested successfully in a vacuum spin chamber for a centrifugal loading of 710g, with no degradation of flap response with rotational speed (up to 1000 RPM) and excitation frequency (up to 6/rev). To achieve reliable flap deflection in a full-scale system, it is important to build a compact bi-directional actuator system of moderate to large force and high stroke capability. The major challenge is to build a compact stroke-amplification system. Overall, this actuation system show the most potential for a full-scale system.

3. Trailing-Edge Flap Actuated with Magnetostrictive Actuators and Extension-Torsion Coupled Composite Tube: To implement the trailing-edge flap concept on a full-scale vehicle, a kevlar-epoxy extension-torsion coupled tube with a magnetostrictive actuator was designed to achieve the desired actuation force and displacement. A piezoelectric stack actuator was found to be better than a magnetostrictive actuator. Ten $[11]_4$ kevlar-epoxy/piezo-stack systems of 20 inch length each in series (placed spanwise) would generate ±5.2 deg of flap deflection. Because of poor structural efficiency of extension-twist coupled structures and with available stack actuators, this actuation system is less meritorious than other actuation systems.

4. Trailing-Edge Flap Actuated with Piezoceramic Actuators and Tailored Bending-Torsion Coupled Composite Tube: This novel actuation system was demonstrated to actuate a trailing-edge flap or an all-movable tip or complete blade twist. For a Froude-scaled model, a flap deflection of ±2 deg at 4/rev was obtained at the operating speed of 875 RPM and there was no degradation of flap amplitude with RPM or with collective setting. For controllable twist configurations, a tip twist of .4 deg at 4/rev was obtained at 875 RPM. For an all-movable 10% tip, a 4-bladed Mach-scaled rotor was successfully tested in hover (RPM = 2000), resulting in tip deflection of ±1.2 to ±1.6 degree (depending on frequency of excitation) with thrust authority of 10% to 30%. From a closed-loop adaptive test, it was demonstrated that this smart tip was capable of minimizing simulated flap bending and rotor thrust by 80% to 95%. This device can be easily accommodated in a blade spar and appears to show the potential to control vibration and acoustics as a partial reduction device in a full-scale system.

5. Controllable Twist Blade with Embedded Piezoceramic Actuators: At an operating speed of 900 RPM in hover, a maximum tip twist of .4 deg at 4/rev was achieved using dual-layer piezoceramics embedded at ±45 deg on the top and bottom surfaces. At an advance ratio of .33, an oscillatory rotor thrust of 11% of nominal steady state value was achieved in a wind tunnel. Using today's actuators technology, it is possible to build a full-scale controllable twist rotor, but at a considerable weight penalty (16% of blade weight). This approach shows the potential for partial vibration suppression

6. Shape Memory Alloy Actuators: The constitutive models of SMA developed by different researchers correlate well with test data as long as the constants the material constants for models are derived properly form test data. Building composite shafts or beams with embedded SMA is a challenge, and needs focused effort. A SMA wire-actuated tab showed deflections of the order of 20 degrees at a forward speed of 120 ft/sec. For in-flight tracking with tab, it is important to incorporate adaptive control strategy and a locking mechanism.

7. Modeling of Blades with Smart Actuators: Validation of newly formulated one-dimensional beam models undergoing bending, extension and torsional deformation with experimental data showed an acceptable correlation for bending response and a poor correlation for torsional response. This beam model needs further refinements to include transverse actuation. Comprehensive aeroelastic analyses for rotors with trailing-edge flaps are under development and need to include the dynamics of smart actuators.

Acknowledgments

Most of these research activities were supported by the Army Research Office under the grants URI: DAAL 03-92-G-0121 and MURI: DAAH-04-96-10334 with Dr. Gary Anderson and Dr. Tom Doligalski as Technical Monitors. Author acknowledges many useful discussions and enthusiastic input from Dr. Friedrich Straub (Boeing-Mesa), Dr. Norman Wereley (UM), Dr. Ramesh Chandra (UM), Darryll Pines (UM) and many graduate students (Peter Chen, Andy Bernhard, Nikhil Koratkar, Jeanette Epps, Taeoh Lee, Jayant Sirohi, Harsha Prahlad, Mike Spencer, Mark Shaner and Judah Milgram).

References

1. Chopra, I., "State-of-the-Art of Smart Structures and Integrated Systems," *Proceedings of the 1996 SPIE's North American Symposium on Smart Structures and Materials,* San Diego, CA, February 1996.

2. Sirohi, J. and Chopra, I., "Fundamental Behavior of Piezoceramic Sheet Actuators," *Proceedings of the 1998 SPIE's North American Symposium on Smart Structures and Materials,* San Diego, CA, March 1998.

3. Sirohi, J. and Chopra, I., "Fundamental Understanding of Piezoelectric Strain Sensors,"

Proceedings of the 1999 SPIE's North American Symposium on Smart Structures and Materials, Newport Beach, CA, March 1999.

4. Epps, J. J. and Chopra, I.,"Compartive Evaluation of Shape Memory Alloy Constitutive Models with Test Data," *Proceedings of the 38th AIAA /ASME/ASCE/AHS/ASC Structures, Structural Dynamics and Materials Conference and Adaptive Structures Forum,* Kissimmee, FL, April 1997.

5. Prahlad, H. and Chopra, I., "Experimental Characterization of Ni-Ti Shape Memory Alloy Wires under Complex Loading Conditions," *Proceedings of the 1999 SPIE's North American Symposium on Smart Structures and Materials,* Newport Beach, CA, March 1999.

6. Samak, D. K. and Chopra, I., "Design of High Force, High Displacement Actuators for Helicopters Rotors" *Smart Materials & Structures*, Vol. 5, No. 1, February 1996, pp. 58-67.

7. Bothwell, C. M., Chandra, R. and Chopra, I., "Torsional Actuation with Extension-Torsional Composite Coupling and Magnetostrictive Actuators," *AIAA Journal,* Vol. 33, No. 4, April 1995, pp. 723-729.

8. Udd, E., "Fiber Optic Sensors: An Introduction for Engineers and Scientists," John Wiley and Sons, New York, 1991.

9. Lee, T. and Chopra, I., "Design and Static Testing of a Trailing-Edge Flap Actuator with Piezostack for a Rotor Blade," *Proceedings of the 1998 SPIE's North American Symposium on Smart Structures and Materials,* San Diego, CA, March 1998.

10. Walz, C. and Chopra, I., "Design and Testing of a Helicopter Rotor Model with Smart Trailing Edge Flaps," *Proceedings of the 35th AIAA /ASME/ASCE/AHS/ASC Structures, Structural Dynamics and Materials Conference and Adaptive Structures Forum,* Hilton Head, SC, April 1994.

11. Chopra, I. and McCloud, J. C., "A Numerical Simulation Study to Open-Loop, Closed-Loop and Adaptive Multicyclic Control Systems," *Journal of the American Helicopter Society,* Vol. 28, No. 1, January 1983, pp. 63-77.

12. Nguyen, K. and Chopra, I., "Application of Higher Harmonic Control to Rotors Operating at High Speed and Thrust," *Journal of the American Helicopter Society,* Vol. 35, No. 3, July 1990, pp. 78-89.

13. Shaw, J., Albion, N., Hanker, E. J. and Teal, R. S.,"Higher-Harmonic Control: Wind Tunnel Demonstration of Fully Effective Vibratory Hub Forces Suppression," *Journal of the American Helicopter Society,* Vol. 34, No. 1, January 1989, pp. 14-25.

14. Wood, E. R., Powers, R. W., Cline, C. H. and Hammond, C. E., " On Developing and Flight Testing a Higher Harmonic Control System," *Journal of the American Helicopter Society,* Vol. 30, No. 1, January 1985, pp. 3-20.

15. Ham, N. D., "Helicopter Individual-Blade Control Research at MIT 1977-1985," *Vertica,* Vol. 11, No. 1/2, 1987, pp. 109-122

16. Richter, P. and Blaas, A., "Full Scale Wind Tunnel Investigation of an Individual Blade Control System for the BO 105 Hingeless Rotor," Proceeding of the 19th European Rotorcraft Forum, Cernobbio (Como), September 1993

17. Jaclin, S. A., Blaas, A., Teves, D. and Kube, R., "Reduction of Helicopter BVI Noise, Vibration, and Power Consumption Through Individual Blade Control," *Proceedings of the 51st Annual Forum of the American Helicopter Society,* Fort Worth, TX, May 1995.

18. Balachandran, B., Sampath, A. and Park, J., "Active Control of Interior Noise in Three-Dimensional Enclosure," *Smart Materials & Structures,* Vol. 5, No. 1, February 1995, pp 89-97.

19. Gembler, W., Schweitzer, H., Maier, R., Pucher M., Janker, P. and Hermle, F., “Smart Struts – The Solution for Helicopter Interior Noise Problem,” Proceeding of the 25th European Rotorcraft Forum, Rome, Italy, September 1999.

20. Crawley, E. F., "Intelligent Structures for Aerospace: A Technology Overview and Assessment," *AIAA Journal*, Vol. 32, No. 8, August 1994, pp. 1689-1699.

21. Wada, B.K., Fanson, J.L., and Crawley, E.F., "Adaptive Structures," *Journal of Intelligent Material Systems and Structurs,* Vol. 1, No. 2, April 1990, pp. 157-174.

22. Ehlers, S. M., and Weisshaar, T. A., "Static Aeroelastic Control of an Adaptive Lifting Surface," *Journal of Aircraft,* Vol. 30, No. 4, July-August 1993, pp. 534-540.

23. Lazarus, K. B., Crawley, E. F. and Bohlmann, J. D., "Static Aeroelastic Control Using Strain Actuated Adaptive Structures," *Journal of Intelligent Material Systems and Structurs,* Vol. 2, No. 3, July 1991, pp. 386-410.

24. Lin, C. Y., Crawley, E. F. and Heeg, J., "Open- and Closed-Loop Results of a Strain-Actuated Active Aeroelastic Wing," *Journal of Aircraft,* Vol. 33, No. 5, September - October 1996, pp. 987-994.

25. Kudva, J., Appa, K., Martin, C., Jardine, P. and Sendeckyi, " Design, Fabrication and Testing of the DARPA/WL "Smart Wing" Wind Tunnel Model," *38th AIAA/ASME/ASCE/AHS/ASC Structures, Structural Dynamics, and Materials* Conference, Kissimmee, Florida, April 1997.

26. Kudva, J. and et al, "Overview of the DARPA/AFRL/NASA Smart Wing Program," *Proceedings of the 1999 SPIE's North American Symposium on Smart Structures and Materials,* Newport Beach, CA, March 1999.

27. Becker, J. and Schroder, "Advanced Aircraft Structures Program: An Overview," *Proceedings of the 1999 SPIE's North American Symposium on Smart Structures and Materials,* Newport Beach, CA, March 1999.

28. Frampton, K. D., Clark, R. L. and Dowell, E. H., "Active Control of Panel Flutter with Piezoelectric Transducers," Journal of Aircraft, Vol. 33, No. 4, July-August 1996, pp. 768-774.

29. Fuller, C. R., Hansen, C. H. and Snyder, S. D., "Experiments on Active Control of Sound Radiation from a Panel Using a Piezoceramic Actuator," *Journal of the Acoustical Society of America,* Vol. 91, No. 6, 1992, pp. 3313-3320.

30. Chopra, I., "Development of a Smart Rotor," Proceeding of the 19th European Rotorcraft Forum, Cernobbio Como, Italy, September 1993.

31. Loewy, R. G., "Recent Developments in Smart Structures with Aeronautical Applications," *Proceedings of the 37th Israel Annual Conference on Aerospace Sciences,* Tel Aviv, Israel, February 1996.

32. Straub, F. K., "A Feasibility Study of Using Smart Materials for Rotor Control" *Smart Materials & Structures,* Vol. 5, No. 1, February 1995, pp 1-10.

33. Straub, F. K. and Merkley, D. J., "Design of a Servo-Flap Rotor for Reduced Control Loads, *Smart Materials & Structures,* Vol. 5, No. 1, February 1995, pp 68-75.

34. Strehlow, H., and Rapp, H., "Smart Materials for Helicopter Rotor Active Control" *Proceedings of AGARD/SMP Specialists Meeting on Smart Structures for Aircraft and Spacecraft,* Lindau, Germany, Oct. 1992.

35. Roglin, R. L. and Hanagud, S. V., "A Helicopter with Adaptive Rotor Blades for Collective Control," *Smart Materials & Structures,* Vol. 5, No. 1, February 1995, pp 1-10.

36. Janker, P., Kloppel, V., Hermle, T., Lorkowski, T., Storm, S., Christmann, M. and Wettemann, "Development and Evaluation of a Hybrid Piezoelectric Actuator for Advanced Flap Control Technology," Proceeding of the 25th European Rotorcraft Forum, Rome, Italy, September 1999.

37. Shaner, M. C. and Chopra, I., "Design and Testing of a Piezostacke Actuated Leading-Edge Flap," *Proceedings of the 1999 SPIE's North American Symposium on Smart Structures and Materials,* Newport Beach, CA, March 1999

38. Kamath, G., Wereley, N. and Jolly, M., "Analysis and Testing of a Model-Scale Magnetorheological Fluid Helicopter Lag Damper," *Proceedings of the 53rd Annual Forum of the American Helicopter Society,* Virginia Beach, VA, May 1997.

39. Pelinescu, I. and Balachandran, B., "Active Control of Vibration Transmission Through Struts," *Proceedings of the 1999 SPIE's North American Symposium on Smart Structures and Materials,* Newport Beach, CA, March 1999.

40. Park, H. and Chopra, I., "Active Control of Airframe Structural Response with Distributed Smart Actuators," Presented at the 4th ARO Smart Structures Workshop, Penn State, August 1999.

41. Wereley, N., "Active and Passive Damping Control of Helicopter Systems," *Proceedings of the 1999 SPIE's North American Symposium on Smart Structures and Materials,* Newport Beach, CA, March 1999.

42. Crawley, E.F., and de Luis, J., "Use of Piezoelectric Actuators as Elements of Intelligent Structures," *AIAA Journal*, Vol. 25, No. 10, Oct. 1987, pp. 1373-1385.

43. Crawley, E. F., and Anderson, E. H., "Detailed Modeling of Piezoceramic Actuation of Beams," *Journal of Intelligent Material Systems and Structures,* Vol. 1, No. 1, Jan. 1990, pp. 4-25.

44. Park, C., Walz, C and Chopra, I., " Bending and Torsion Models of Beams with Induced-Strain Actuators," *Smart Materials & Structures,* Vol. 5, No. 1, February 1995, pp 98-113.

45. Park, C. and Chopra, I., " Modeling of Piezoceramic Actuation of Beams in Torsion," *AIAA Journal,* Vol. 34, No. 12, December 1996, pp 2582-2589.

46. Koratkar, N. and Chopra, I., "Analysis and Testing of Mach Scaled Rotor Model with Piezoelectric Bender Actuated Trailing-Edge Flaps for Helicopter Vibration Control,"*Proceedings of the 38th AIAA /ASME/ASCE/AHS/ASC Structures, Structural Dynamics and Materials Conference and*

Adaptive Structures Forum, St. Louis, MO, April 1999.

47. Samak, D. K., and Chopra, I., "A Feasibility Study to Build a Smart Rotor: Trailing Edge Flap Actuation" *Proceedings of the 1993 SPIE's North American Symposium on Smart Structures and Materials,* Albuquerque, NM, February 1993.

48. Ben-Zeev, O. and Chopra, I., "Advances in the Development of an Intelligent Helicopter Rotor Employing Smart Trailing-Edge Flaps," *Smart Materials & Structures*, Vol. 5, No. 1, February 1996, pp. 11-25.

49. Koratkar, N. A., and Chopra, I., "Analysis and Testing of a Froude Scaled Helicopter Rotor with Piezoelectric Bender Actuated Trailing Edge Flaps," *Journal of Intelligent Material Systems and Structures,* Vol. 8, July 1997, pp. 555-570.

50. Hariharan, N. and Leishman, J. G., "Unsteady Aerodynamics of Flapped Airfoil in Subsonic Flow by Indicial Concepts," *Journal of Aircraft,* Vol. 33, No. 5, Sept.-Oct., 1996, pp. 855-868.

51. Koratkar, N. A., and Chopra, I., "Design, Fabrication and Testing of a Mach Scaled Rotor Model with Trailing-Edge Flaps," *Proceedings of the 55th Annual Forum of the American Helicopter Society,* Montreal, Canada, May 1999.

52. Koratkar, N. A. and Chopra, "Wind Tunnel Testing of a Mach-Scaled Rotor Model with Trailing-Edge Flaps," *Proceedings of the 56th Annual Forum of the American Helicopter Society,* Virginia Beach, VA, May 2000.

53. Spangler, R.L., and Hall, S.R., "Piezoelectric Actuators for Helicopter Rotor Control," *Proceedings of the 31st AIAA /ASME/ASCE/AHS/ASC Structures, Structural Dynamics and Materials Conference,* Long Beach, CA, April 1990.

54. Hall, S.R. and Prechtl, E. F., "Development of a Piezoelectric Servoflap for Helicopter Rotor Control," *Smart Materials & Structures*, Vol. 5, No. 1, February 1996, pp. 26-34.

55. Fulton, M. V. and Ormiston, R. A., "Hover Testing of a Small-Scale Rotor with On-Blade Elevons" *Proceedings of the 53rd Annual Forum of the American Helicopter Society,* Virginia Beach, VA, May 1997.

56. Fulton, M. V. and Ormiston, R. A., "Small-Scale Rotor Experiments with On-Blade Elevons to Reduce Blade Vibratory Loads in Forward Flight," *Proceedings of the 54th Annual Forum of the American Helicopter Society,* Washington, DC, May 1998.

57. Spencer, B. and Chopra, I., "Advances in the Development of an Intelligent Helicopter Rotor Employing Smart Trailing-Edge Flaps," *Proceedings of the 1996 SPIE's North American Symposium on Smart Structures and Materials,* San Diego, CA, February 1996.

58. Chandra, R. and Chopra, I. "Actuation of Trailing Edge Flap in Wing Model Using Piezostack Device," *Proceedings of the 38th AIAA /ASME/ASCE/AHS/ASC Structures, Structural Dynamics and Materials Conference and Adaptive Structures Forum,* Kissimmee, FL, April 1997.

59. Lee, T. and Chopra, I., "Design and Spin Testing of an Active Trailing Edge Flap Actuated Piezostacks," Proceedings of the *AIAA /ASME/ASCE/AHS/ASC Structures, Structural Dynamics and Materials Conference and Exhibit,* St. Louis, MO, April 1999.

60. Lee, T. and Chopra, I., "Development and Validation of a Refined Piezostack-Actuated Trailing Edge Flap Actuator for a Helicopter Rotor," *Proceedings of the 1999 SPIE's North American Symposium on Smart Structures and Materials,* Newport Beach, CA, March 1999.

61. Lee, T., "High Displacement Piezoelectric Trailing-Edge Flap Mechanism for Helicopter Rotors," Ph.D. Dissertation, University of Maryland, College Park, MD, December 1999.

62. Straub, F. K. and King, R. J., "Application of Smart Materials to Control of a Helicopter Rotor," *Proceedings of the 1996 SPIE's North American Symposium on Smart Structures and Materials,* San Diego, CA, February 1996.

63. Straub, F. K., Ealey, M. A. and Schetky, L. M., "Application of Smart Materials to Helicopter Rotor Active Control,"*Proceedings of the 1997 SPIE's North American Symposium on Smart Structures and Materials,* San Diego, CA, March 1997.

64. Straub, F. K. and Hassan, A. A., "Aeromechanic Considerations in the Design of a Rotor with Smart Material Actuated Trailing Edge Flaps," *Proceedings of the 52nd Annual Forum of the American Helicopter Society,* Washington D.C., June 1996

65. Straub, F. K., Ngo, H. T., Anand, V. and Domzalski, D. B., "Development of a Piezoelectric Actuator for Trailing Edge Flap Control of Rotor Blades," *Proceedings of the 1999 SPIE's North American Symposium on Smart Structures and Materials,* Newport Beach, CA, March 1999.

66. Prechtl, E. F. and Hall, S. R., "Design of a High-Efficiency Discrete Servo-Flap Actuator for Helicopter Rotor Control," *Proceedings of*

the 1997 SPIE's North American Symposium on Smart Structures and Materials, San Diego, CA, March 1997.

67. Hall, S. R. and Prechtl, E. F., "Preliminary Testing of a Mach-Scaled Active Rotor Blade with a Trailing Edge Servo-Flap,"*Proceedings of the 1999 SPIE's North American Symposium on Smart Structures and Materials,* Newport Beach, CA, March 1999.
68. Schimke, D., Janker, P., Blaas, A., Kube, R. and Kessler, C. "Individual Blade Control by Servo-Flap and Blade Root Control A Collaborative Research and Development Programme," Proceedings of the European Rotorcraft Forum, Dresden, Germany, September 1997.
69. Schimke P., Janker, V., Wendt, V. and Junker, B., "Wind Tunnel Evaluation of a Full Scale Piezoelectric Flap Control Unit, Proceedings of the European Rotorcraft Forum, Marseille, France, September 1998.
70. Shaner, M., "Active Blade Leading-Edge Droop with Piezostacks for High Speed Noise Suppression," MS Thesis, University of Maryland, College Park, January 2000.
71. Chandra, R. and Chopra, I., "Structural Response of Composite Beams and Blades with Elastic Couplings," *Composite Engineering,* Vol. 2, No. 5, 1992, pp. 347-374.
72. Bernhard, A., Chopra, I., "Trailing Edge Flap Activated by a Piezo-Induced Bending-Torsion Coupled Beam", Journal of the American Helcopter Society, Vol. 44, No. 1, January 1999, pp. 3-15.
73. Bernhard, A., Chopra, I., "Development of a Smart Moving Blade Tip Activated by a Piezo-Induced Bending-Torsion Coupled Beam", *Proceedings of the 1996 SPIE's North American Symposium on Smart Structures and Materials,* San Diego, CA, February 1996.
74. Bernhard, A., Chopra, I., "Development of a Smart Moving Blade Tip by a Piezo-Induced Bending-Torsion Coupled Beam", *Proceedings of the 53rd Annual Forum of the American Helicopter Society,* Virginia Beach, VA, May 1997.
75. Bernhard, A., Chopra, I., "Mach-Scale Design of a Rotor-Model with Active Blade Tip", *Proceedings of the 55th Annual Forum of the American Helicopter Society,* Montreal, Canada, May 1999.
76. Bernhard, A., "Smart Helicopter Rotor with Active Blade Tips (SABT)," Ph. D. Dissertation, Aerospace Engineering, University of Maryland, March 2000.
77. Chen, P. C., and Chopra, I., "A Feasibility Study Build a Smart Rotor: Induced-Strain Actuation of Airfoil Twisting Using Piezoelectric Crystals" *Proceedings of the 1993 SPIE's North American Symposium on Smart Structures and Materials,* Albuquerque, NM, February 1993.
78. Chen, P. C. and Chopra, I., "Induced Strain Actuation of Composite Beams and Rotor Blades with Embedded Piezoceramic Elements," *Smart Materials & Structures*, Vol. 5, No. 1, February 1996, pp. 35-48.
79. Chen, P. C. and Chopra, I., "Hover Testing of Smart Rotor with Induced-Strain Actuation of Blade Twist," AIAA Journal, Vol. 35, No. 1, January 1997, pp. 6-16.
80. Chen, P. C. and Chopra, I., "Wind Tunnel Test of a Smart Rotor with Individaul Blade Twist Control," Journal of Intelligent Material Systems and Structures, Vol. 8, No. 5, May 1997, pp. 414-425.
81. Chen, P. C., "Development of a Smart Rotor with Induced-Strain Actuation of Blade Twist," Ph. D. Dissertation, Aerospace Engineering, University of Maryland, 1996.
82. Rodgers, J. P. and Hagood, N. W., "Design and Manufacture of an Integral Twist-Actuated Rotor Blade,"*Proceedings of the 38th AIAA /ASME/ASCE/AHS/ASC Structures, Structural Dynamics and Materials Conference and Adaptive Structures Forum,* Kissimmee, FL, April 1997.
83. Derham, R. C. and Hagood, N. W., "Rotor Design Using Smart Materials to Actively Twist Blades,"*Proceedings of the 52nd Annual Forum of the American Helicopter Society,* Washington, DC, June 1996.
84. Rogers, J. P. and Hagood, N. W., "Preliminary Mach-Scale Hover Testing of an Integral Twist-Actuated Rotor Blade,"*Proceedings of the 1997 SPIE's North American Symposium on Smart Structures and Materials,* San Diego, CA, March 1997.
85. Rogers, J. P. and Hagood, N. W., "Development of an Integral Twist-Actuated Rotor Blade for Individual Blade Control,"*MIT AMSL 98-6* , October 1998.
86. Tanaka, K., "A Thermomechanical Sketch of Shape Memory Effect: One-dimensional Tensile Behavior," *Res. Mechanica*, Vol. 18, p. 251-263, 1986.
87. Liang, C., and Rogers, C. A., "One-Dimensional Thermomechanical Constitutive Relations for Shape Memory Material," *Journal of Intelligent Materials and Structures*, Vol. 1, April 1990, pp. 207-234.

88. Brinson, L. C., "One Dimensional Constitutive Behavior of Shape Memory Alloys: Thermo-mechanical Derivation with Non-Constant Material Functions," *Journal of Intelligent Material Systems and Structures* Vol. 4, No. 2, p. 229-242, 1993.

89. Boyd, J. G., and Lagoudas, D. C., "A thermodynamic Constitutive Model for the Shape Memory Materials. Part I. The Monolithic Shape Memory Alloys," *International Journal of Plasticity*, Vol. 12, No. 6, 1996, pp. 805-842.

90. Rogers, C. A., Liang, C., and Jia, J., "Behavior of Shape Memory Alloy Reinforced Composite Plates, Part I: Model Formulations and Control Concepts,"*Proceedings of the 30th AIAA/ASME/ASCE/AHS/ASC Structures, Structural Dynamics and Materials Conference,* Washington D.C., April 1989.

91. Rogers, C. A., Liang, C., and Jia, J., "Behavior of Shape Memory Alloy Reinforced Composite Plates, Part II: Results,"*Proceedings of the 30th AIAA/ASME/ASCE/AHS/ASC Structures, Structural Dynamics and Materials Conference,* Washington D.C., April 1989.

92. Rogers, C. A., and Barker, D. K., "Experimental Studies of Active Strain Energy Tuning of Adaptive Composites,"*Proceedings of the 31st AIAA/ASME/ASCE/AHS/ASC Structures, Structural Dynamics and Materials Conference,* Washington D.C., April 1990.

93. Baz, A., Imam, K., McCoy, J., "Active Vibration Control of Flexible Beams Using Shape Memory Actuators," *Journal of Sound and Vibration*, Vol. 140 (3), 1990, pp. 437-456.

94. Baz, A. and Ro, S., " Thermo-Dynamic Characteristics of Nitinol-Reinforced Composite Beams," *Composite Engineering,* Vol. 2, No. 5-7, 1992, pp. 527-542.

95. Epps, J. J., and Chandra, R., "Shape Memory Alloy Actuation for Active Tuning of Composite Beams," *Proceedings of the 1995 SPIE's North American Symposium on Smart Structures and Materials,* San Diego, CA, February 1995.

96. Epps, J. J., and Chandra, R., "Shape Memory Alloy Actuation for Active Tuning of Composite Shafts," *Proceedings of the 1996 SPIE's North American Symposium on Smart Structures and Materials,* San Diego, CA, February 1996.

97. Liang, C., Schroeder, S. and Davidson, F. M., "Application of Torsion Shape Memory Alloy Actuators for Active Rotor Blade Control: Oportunities and Limitations," *Proceedings of the 1996 SPIE's North American Symposium on Smart Structures and Materials,* San Diego, CA, February 1996.

98. Straub, F. K., Ealey, M. A., and Schetky, L.McD., "Application of Smart Materials to Helicopter Active Control," *Proceedings of the 1997 SPIE's North American Symposium on Smart Structures and Materials,* San Diego, CA, March 1997.

99. Epps, J. J. and Chopra, I., "Shape Memory Alloy Actuators for In-Flight Tracking of Helicopter Rotor Blades," *Proceedings of the 1998 SPIE's North American Symposium on Smart Structures and Materials,* San Diego, CA, March 1998.

100. Epps, J. J. and Chopra, I., "In-Flight Tracking of Helicopter Rotor Blades Using Shape Memory Alloy Actuators," *Proceedings of the 40th AIAA /ASME/ASCE/AHS/ASC Structures, Structural Dynamics and Materials Conference and Adaptive Structures Forum,* St. Louis, MO, April 1999.

101. Epps, J. J. and Chopra, I., "Methodology of In-Flight Tracking of Helicopter Rotor Blades Using Shape Memory Alloy Actuators," *Proceedings of the 55th Annual Forum of the American Helicopter Society*, Virginia Beach, VA, May 1999.

102. Epps, J. J., "In-Flight Tracking of Helicopter Rotor Blades with Tabs actuated with Shape Memory Alloy Actuators," Ph. D. Dissertation, Aerospace Engineering, University of Maryland, Feb. 2000.

103. Chandra, R. and Chopra, I., "Structural Modeling of Composite Beams with Induced Strain Actuation," *AIAA Journal,* Vol. 31, No. 9, Sept. 1993, pp. 1692-1701.

104. Milgram, J. and Chopra, I., "A Comprehensive Rotorcraft Aeroelastic Analysis with Trailing-Edge Flaps: Validation with Experimental Data, *Proceedings of the 52nd Annual Forum of the American Helicopter Society*, Washington D.C., June 1996.

105. Milgram, J., Chopra, I. and Straub, F., "Rotors with Trailing Edge Flaps: Analysis and Comparison with Experimental Data," *Journal of the American Helicopter Society,* Vol. 43, No. 4, October 1998, pp. 319-332.

106. Hariharan, N. and Leishman, J. G., "Unsteady Aerodynamics of a Flapped Airfoil in Subsonic Flow by Indicial Concepts," Journal of Aircraft, Vol. 33, No. 5, Sept.-Oct. 1996, pp. 855-868.

107. Bagai, A. and Leishman, J. G., "Rotor Free-Wake Modeling Using a Pseudo-Implicit Technique – Including Comparisons with Experimental Data," *Journal of the American*

Helicopter Society, Vol. 40, No. 3, July 1995, pp.

108. Milgram, J. and Chopra, I. "A Parametric Design Study for Actively Controlled Trailing Edge Flaps," *Journal of the American Helicopter Society,* Vol. 43, No. 2, April 1998, pp. 110-119.

109. Milgran, J., "A Comprehensive Aeroelastic Analysis of Helicopter Main Rotors with Trailing Edge Flaps for Vibration Reduction," Ph. D. Dissertation, Aerospace Engineering, University of Maryland, 1997.

110. Millott, T. A. and Friedmann, P. P., "The Practical Implementation of an Actively Controlled Flap to Reduce Vibration in Helicopter Rotors," *Proceedings of the 49th Annual Forum of the American Helicopter Society*, St. Louis, MO, May 1993.

111. Millott, T. A. and Friedmann, P. P., "Vibration Reduction in Hingeless Rotors Using an Actively Controlled Trailing Edge Flap: Implementation and Time Domain Simulation," *Proceedings of the 35th AIAA /ASME/ASCE/AHS/ASC Structures, Structural Dynamics and Materials Conference and Adaptive Structures Forum,* Hilton Head, SC, April 1994.

112. Myrtle, T. F. and Friedmann, P. P., "Vibration Reduction in Rotorcraft Using Actively Controlled Trailing Edge Flaps and Issues Related to Practical Implementation," *Proceedings of the 54th Annual Forum of the American Helicopter Society*, St. Louis, Washington, D. C., May 1998.

113. Myrtle, T. F. and Friedmann, P. P., "New Comprehensive Time Domain Unsteady Aerodynamics for Flapped Airfoils and Its Application to Rotor Vibration Reduction Using Active Control," *Proceedings of the 53rd Annual Forum of the American Helicopter Society*, Virginia Beach, VA, May 1997.

114. Straub, F. K. and Hasan, A. A., "Aeromechanic Consideration in the Design of a Rotor with Smart Material Actuated Trailing Edge Flaps," *Proceedings of the 52nd Annual Forum of the American Helicopter Society,* Washington D. C., June 1996.

115. Straub, F. K. and Charles, B. D., "Comprehensive Modeling of Rotors with Trailing Edge Flaps," *Proceedings of the 55th Annual Forum of the American Helicopter Society,* Montreal, Canada, May 1999.

116. Shen, J. and Chopra, I., "Aeroelastic Modeling of Trailing-Edge Flaps with Smart Material Actuators," ," *Proceedings of the 41st AIAA /ASME/ASCE/AHS/ASC Structures, Structural Dynamics and Materials Conference and Adaptive Structures Forum,* Atlanta, GA, April 2000.

Part/material No.	Operating voltage *V*	Maximum Strain *μ-strain*	Block force (BF) *lbs.*	Normalized Block force ksi	Strain-force index	Energy Density *ft-lb/slug*
MM 8M (70018)	360	254	128	1.05	0.133	1.27
MM 5H (70023-1)	200	449	101	0.83	0.180	1.80
MM 4S (70023-2)	360	497	143	1.17	0.291	2.78
PI P-804.10	100	1035	1133	7.31	3.783	36.72
PI PAH-018.102	1000	1358	1505	9.71	6.593	62.95
XI RE0410L	100	468	95	5.16	1.207	11.52
XI PZ0410L	100	910	70	3.58	1.629	15.55
EDO 100P-1 (98)	800	838	154	2.00	0.838	8.00
EDO 100P-1 (69)	800	472	50	0.66	0.156	1.49
SU 15C (H5D)	150	940	266	7.48	3.516	33.57
SU 15C (5D)	150	1110	274	7.70	4.274	40.80

Table 1: Comparative test evaluation of commercially available piezostack actuators

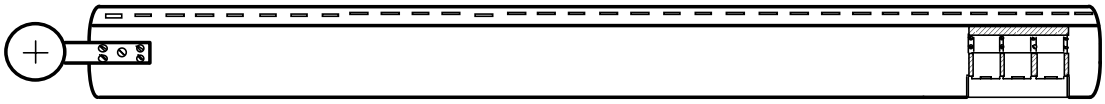

MAIN ROTOR BLADE WITH FLAP ACTUATOR

Fig. 1 (a)

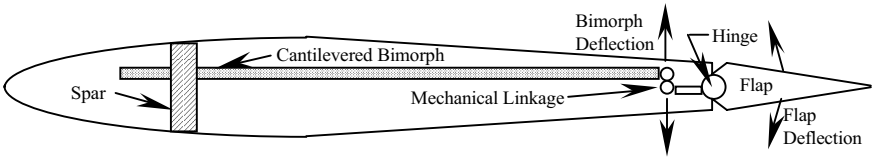

Fig. 1(b): Actuator layout in blade section

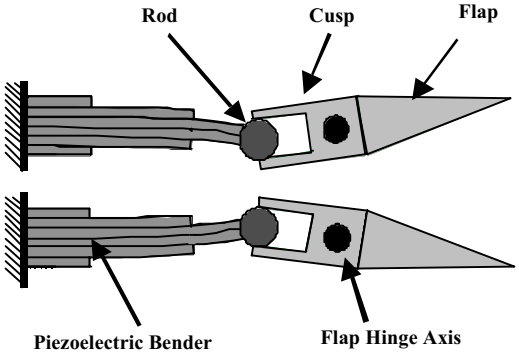

Fig. 2: Piezo-bimorph flap actuation system

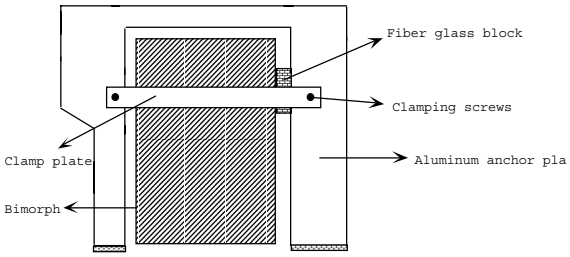

Fig.3: Bimorph clamping arrangement

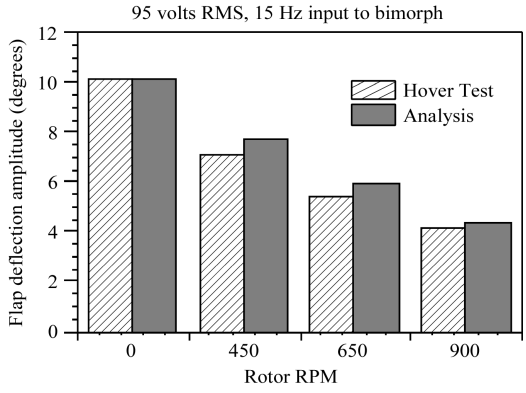

Fig, 4: Froude scaled rotor model in hover: RPM sweep with 1/rev excitation [45]

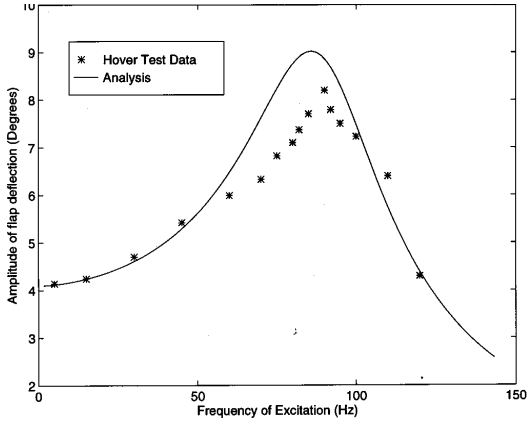

Fig. 5: Froude scaled rotor model in hover: frequency sweep at 900 RPM [45]

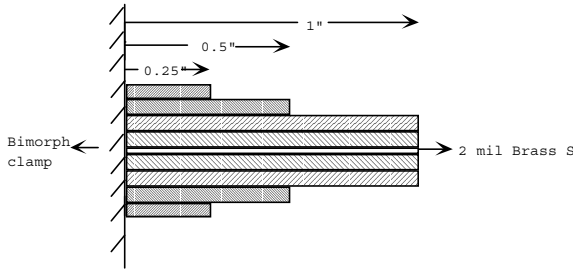

Fig. 6: 8-layered, one inch wide, tapered Piezo-Bimorph (each PZT layer is 7.5 mils thick) [45]

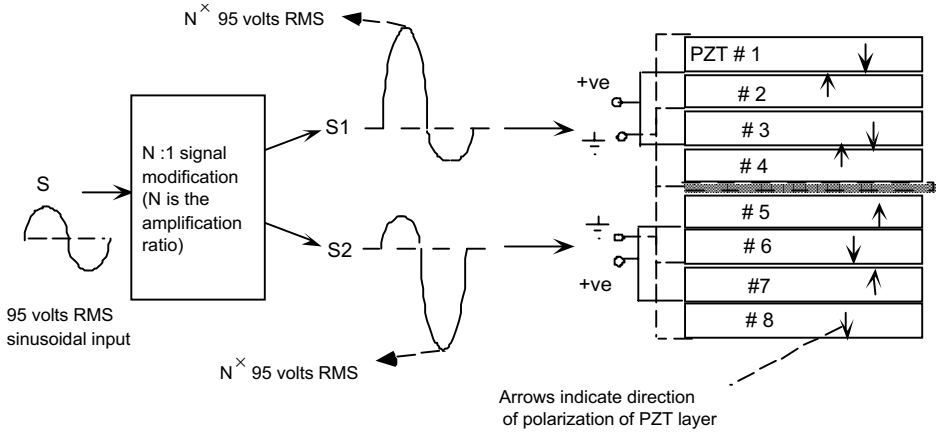

Fig. 7: AC bias circuit

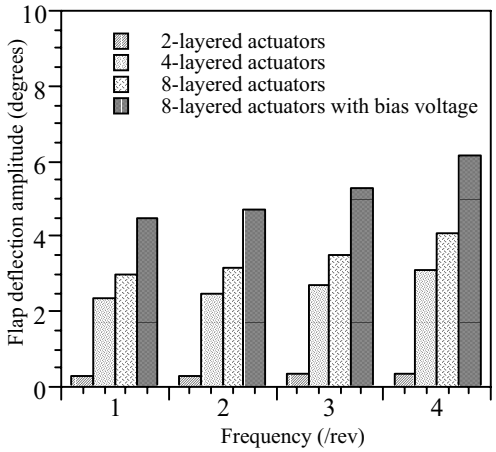

Fig. 8: Comparison of actuator configurations for Mach scaled rotor [45]

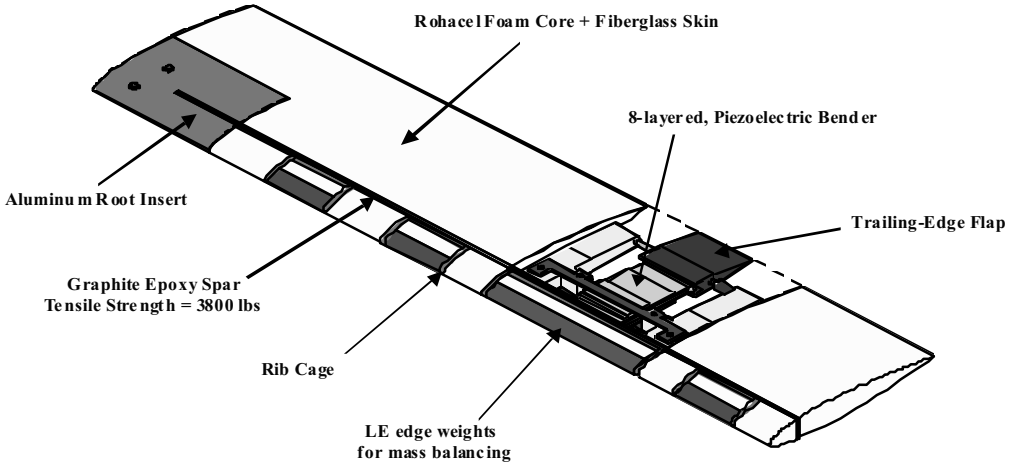

Fig. 9: Mach scaled blade layout

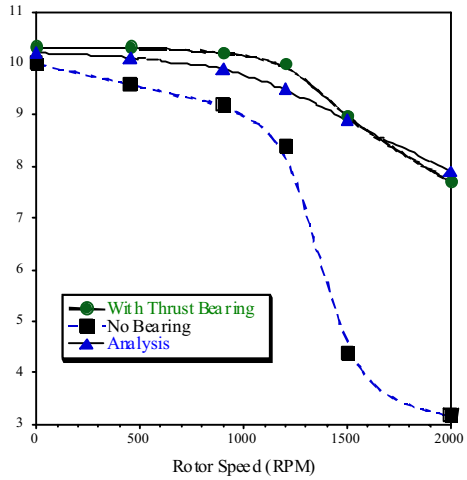

Fig. 10: Mach scaled rotor test in vacuum chamber: with and without thrust bearing and correlation with predictions [51]

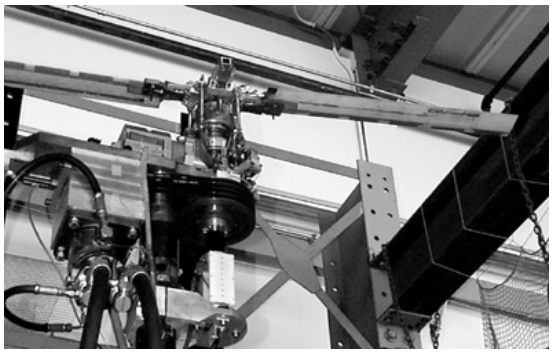

Fig. 11: Model rotor test on a hover stand

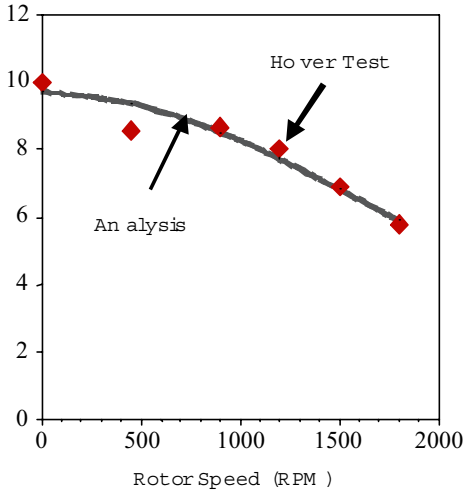

(a) RPM sweep with 1/rev excitation

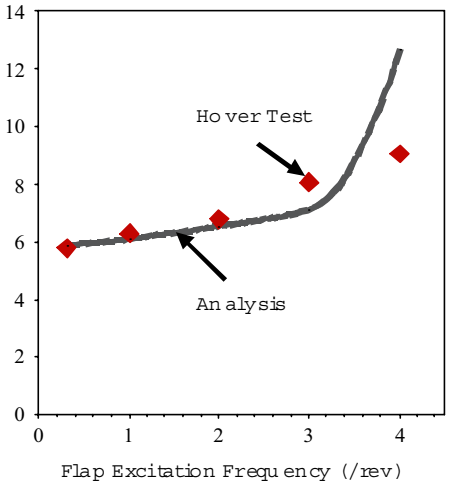

(b) Frequency sweep at 1850 RPM

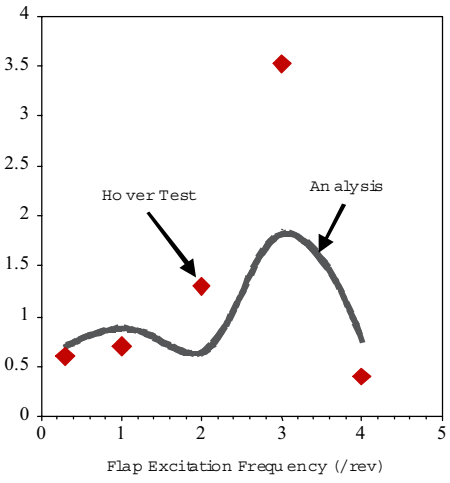

(c) Oscillatory rotor thrust due to 1/rev excitation

Fig. 12: Mach scaled rotor test in hover: at 1850 RPM [52]

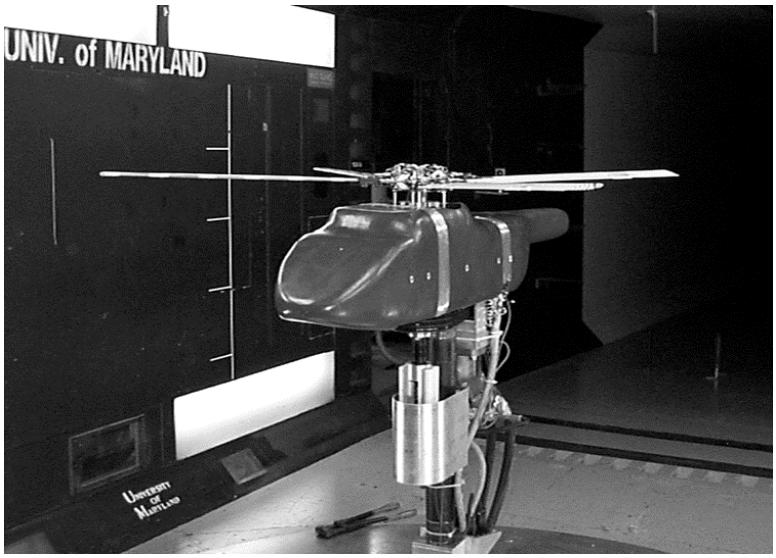

Fig. 13 Mech-scaled rotor model in the Glenn L. Martin wind tunnel

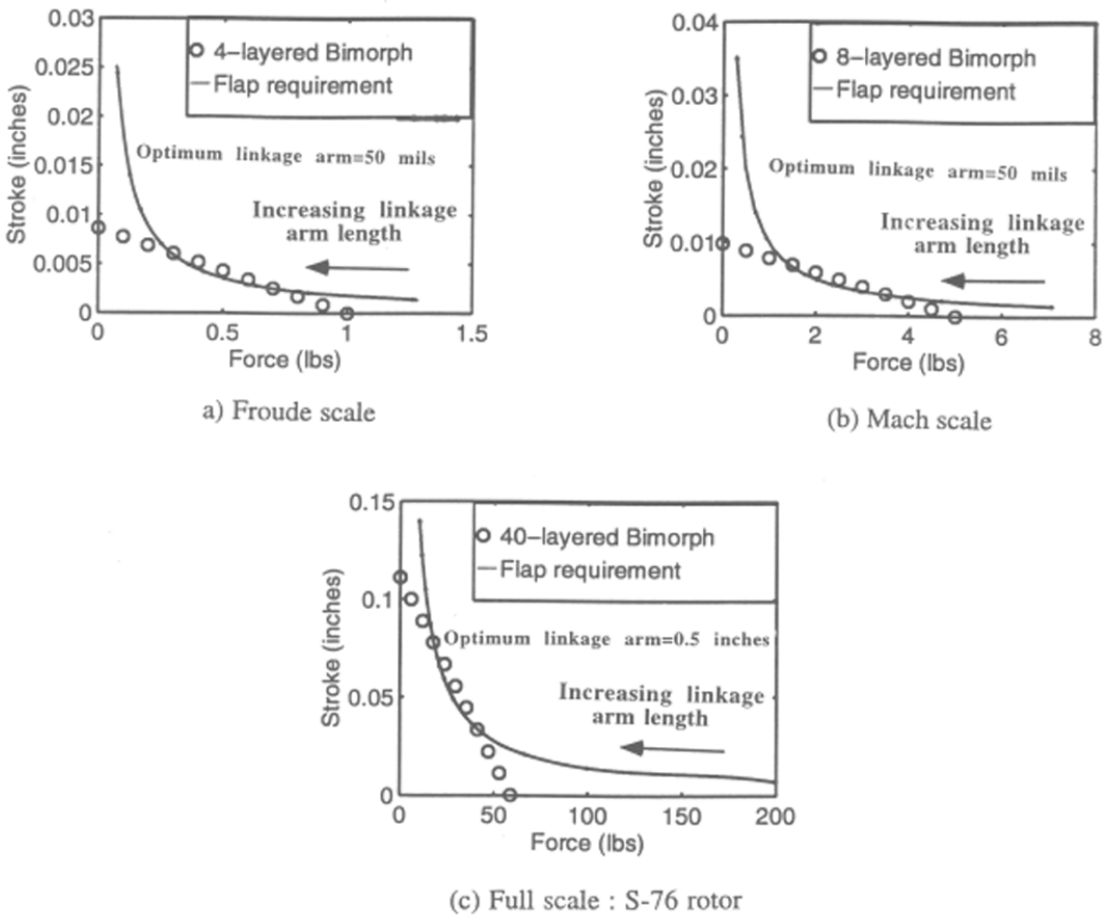

Fig. 14: Actuator capability (14.5 Vrms/mil) vs flap requirements (8 degrees peak to peak deflection) for a 5% span, 20% chord flap located at 75% radius

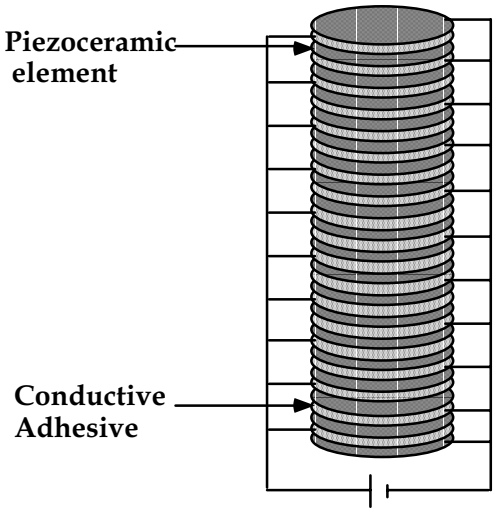

Figure 15. Schematic of a typical piezostack actuator

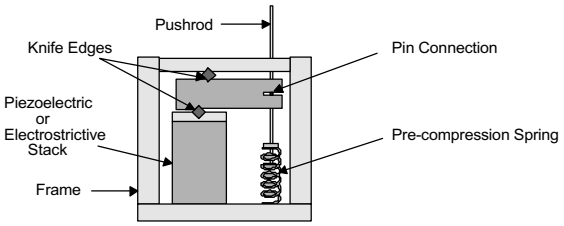

Fig. 16: Mechanical leverage amplification system [6].

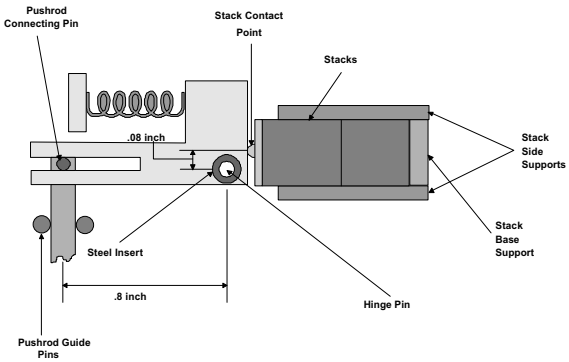

Fig. 17: Stacks and L-Arm Arrangement [57]

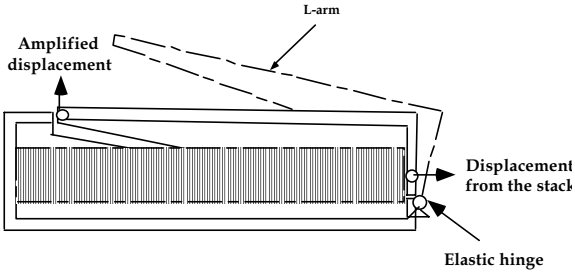

Fig. 18: Piezostack Actuator with Integrated Mechanical Amplification

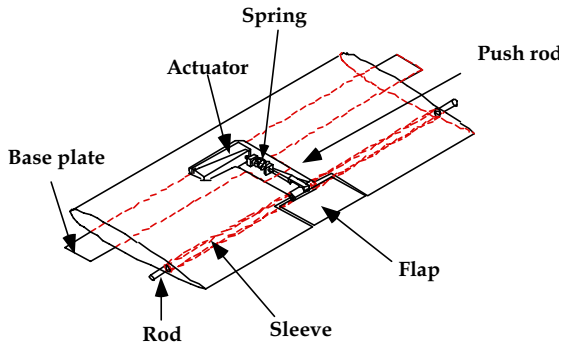

Fig. 19: Schematic of wing model with flap actuated with piezo stack and flexural amplification [58]

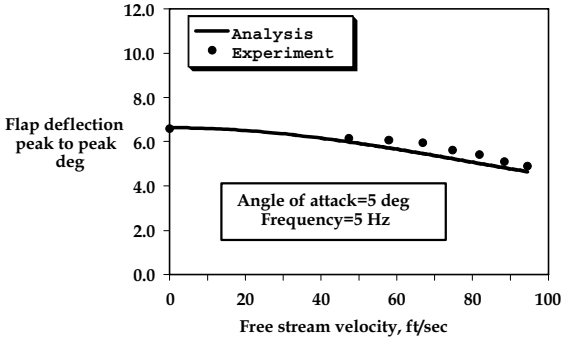

Fig. 20: Flap deflection at 5 Hz frequency, 5 deg angle of attack [58]

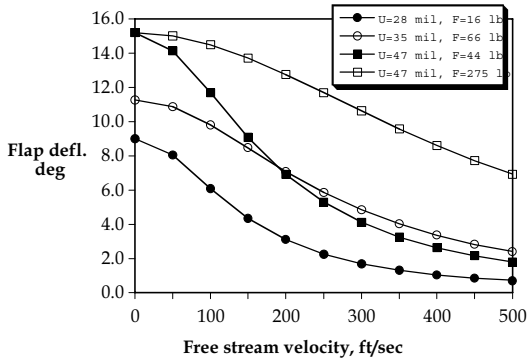

Fig. 21: Predicted flap amplitude at different speeds with four different piezostack actuators [58]

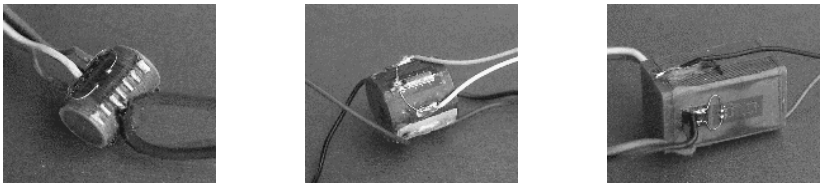

EDO Morgan Matroc (MM) Physik Instrumente (PI)

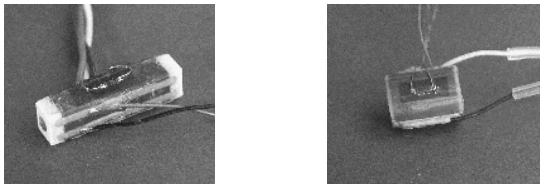

Sumitomo (SU) Xinetics (XI)

Fig. 22: Piezostack actuators

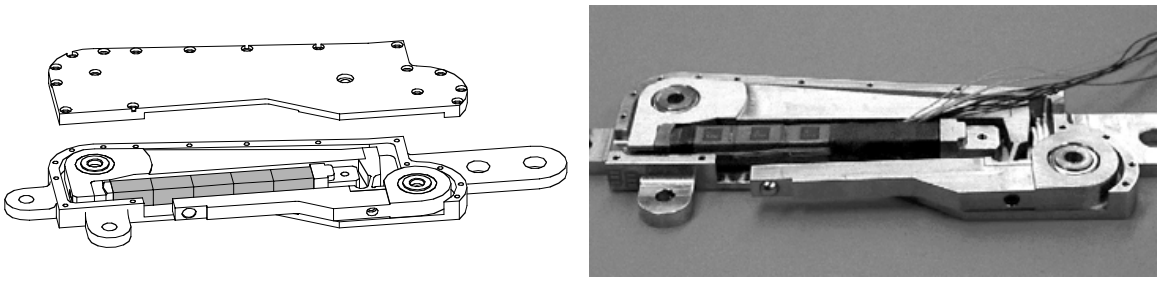

(a) Actuator lay-out (b) Fabricated actuator

Fig. 23: Flap actuator with L-L amplification mechanism [60]

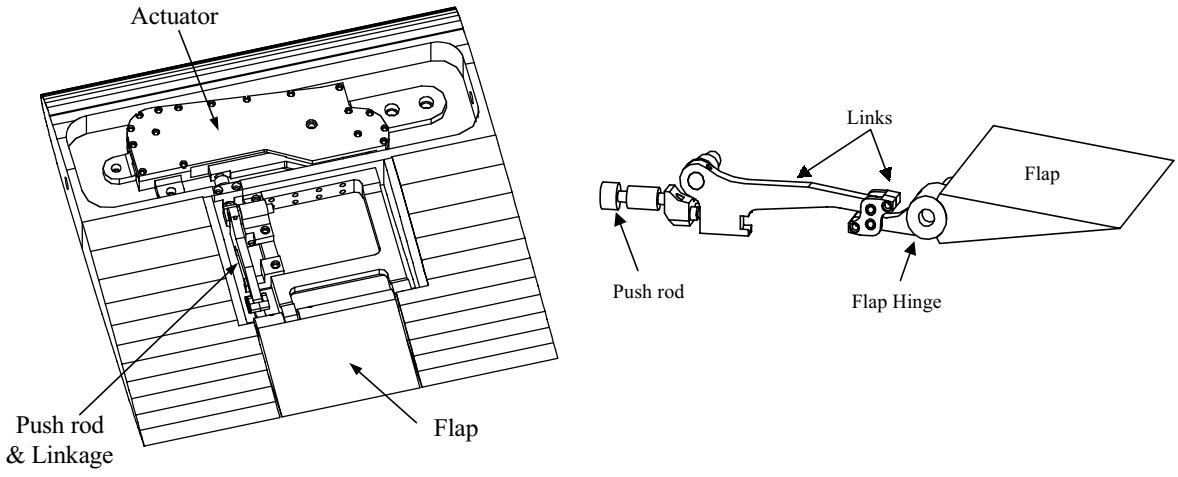

(a) Wing lay-out (b) Flap/actuator push-rod attachment

Fig. 24: Model wing section with trailing-edge flap actuated with piezostacks in conjunction with L-L amplification mechanism [60]

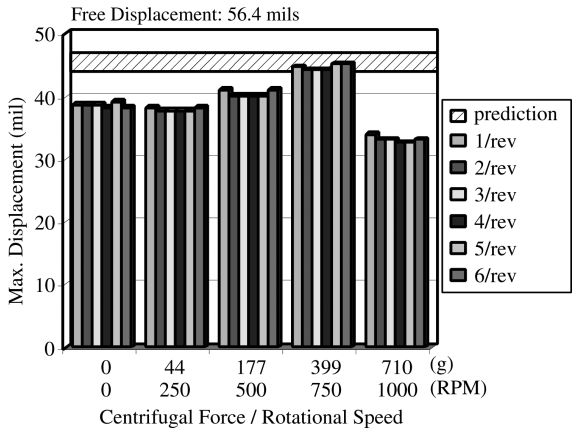

Fig. 25: Vacuum spin testing of L-L actuator: actuator stroke vs. CF loading (90Vpp excitation) [59]

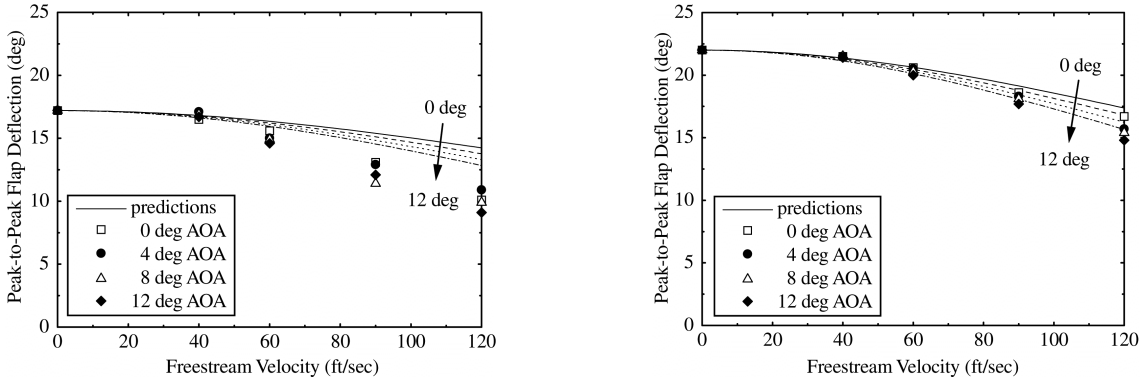

Fig. 26: Peak-to-peak flap deflection vs. freestream velocity for the excitation frequencies of: (a) 1/rev (6.53Hz) and (b) 2/rev (13.1Hz) (90Vpp excitation) [61]

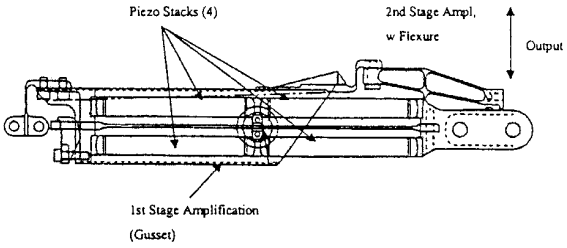

Fig. 27: Bi-axial piezostack flap actuator schematic [65]

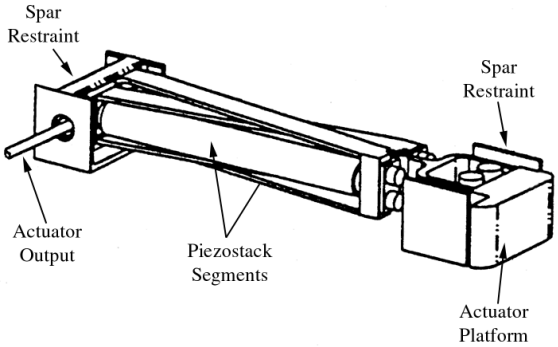

Fig. 28: X-Frame actuator schematic [67]

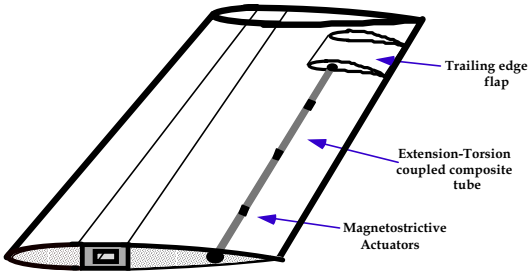

Fig. 29: Schematic of rotor blade trailing edge flap actuated by extension-torsion coupled composite tube and magnetostrictive actuators [7]

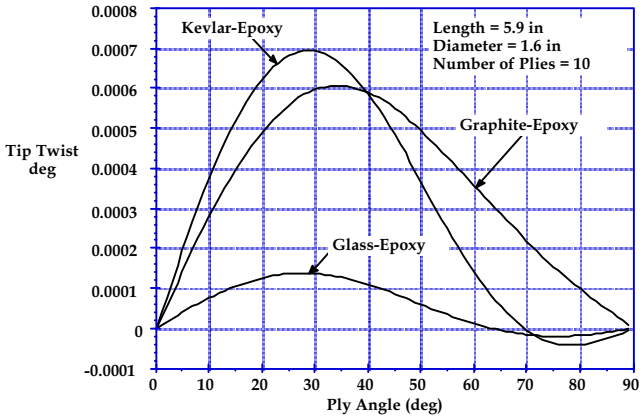

Fig. 30: Induced Twist vs. ply angle for extension-torsion composite tube for a Prescribed Axial Load [7]

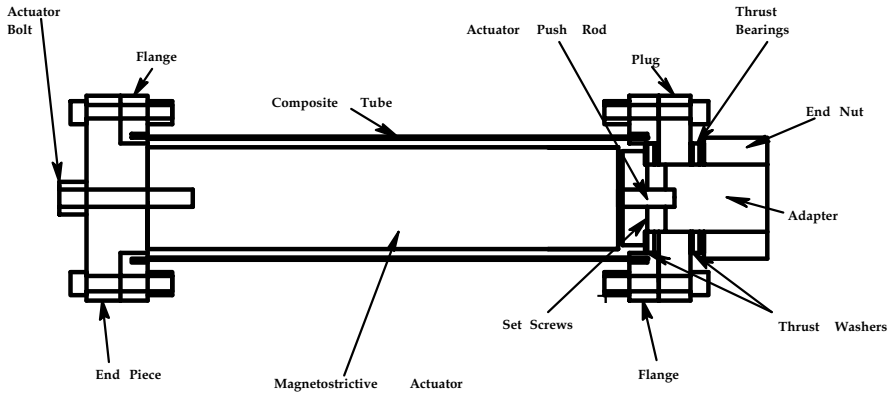

Fig. 31: Schematic of composite tube and actuator assembly [7]

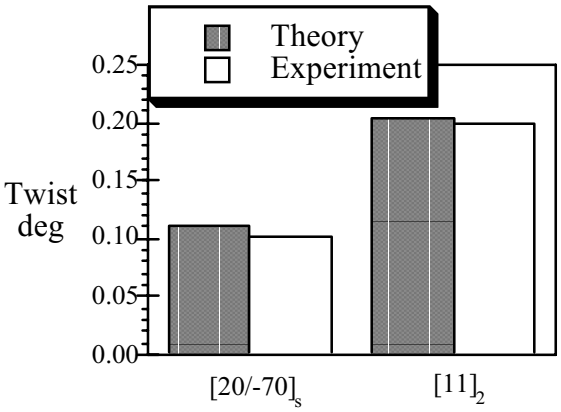

Fig. 32 (a): Tip Twist of Kevlar-Epoxy Tube with Extension-Torsion & Manetostrictive Actuator [7]

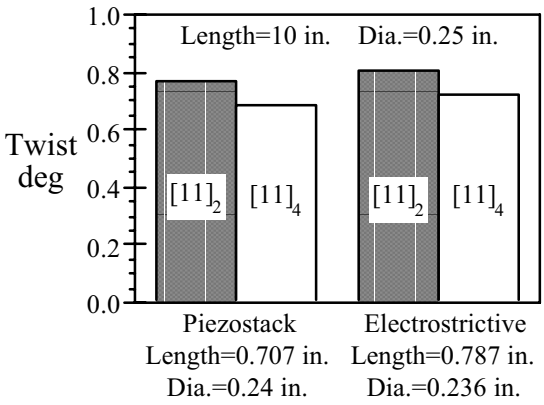

Fig. 32 (b): Tip Twist of Kevlar-Epoxy Tube with Piezoelectric and Electrostrictive Stacks [7]

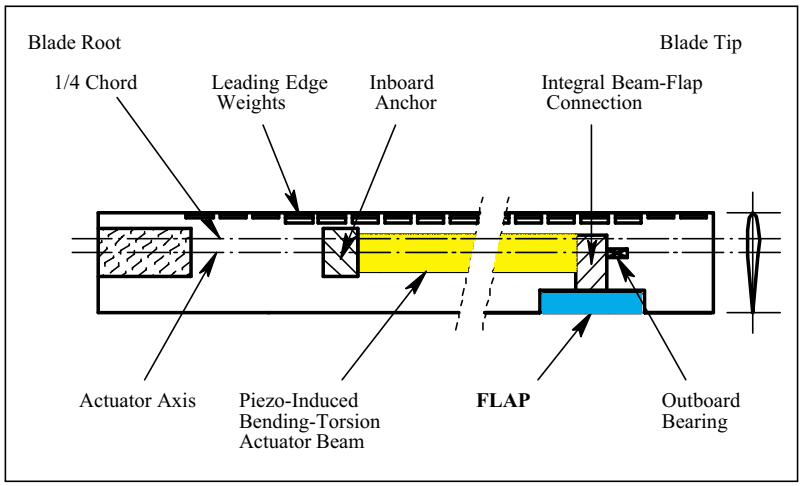

Fig. 33: Trailing-Edge Flap Actuated with Bending-Torsion Actuator

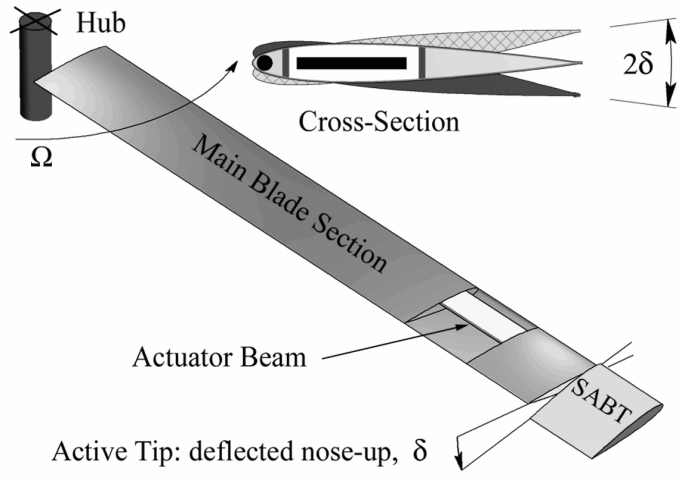

Fig. 34 Blade tip actuated with bending-torsion actuator [73]

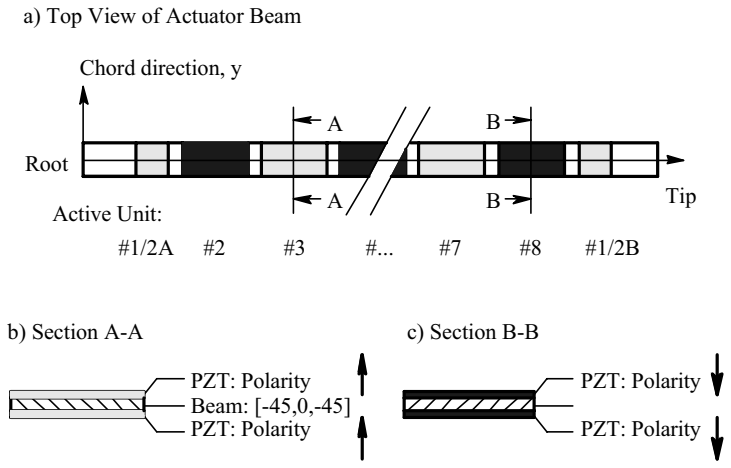

Fig. 35: Composite Bending-Torsion Beam [72]

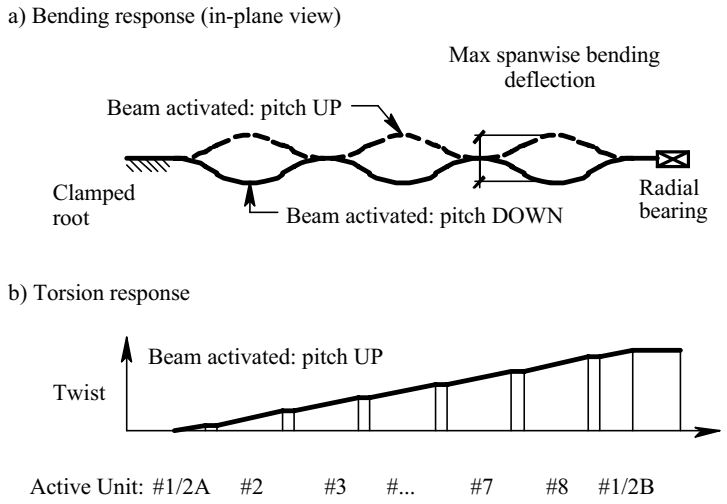

Fig. 36: Schematic of Actuator Beam Mechanics [72]

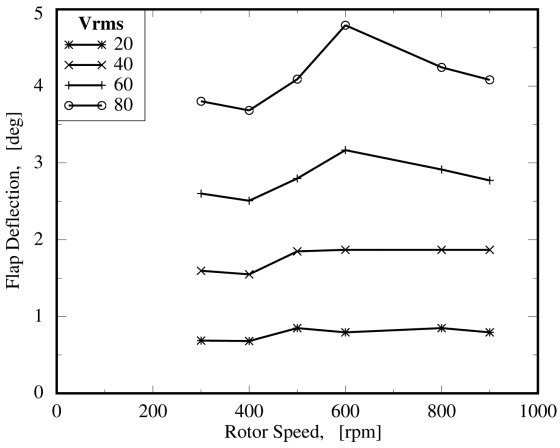

Fig. 37: Hover Test Results: Trailing-Edge Flap, Peak-to-Peak Flap Deflection, Zero Collective, Excitation Frequency = 40 Hz [72]

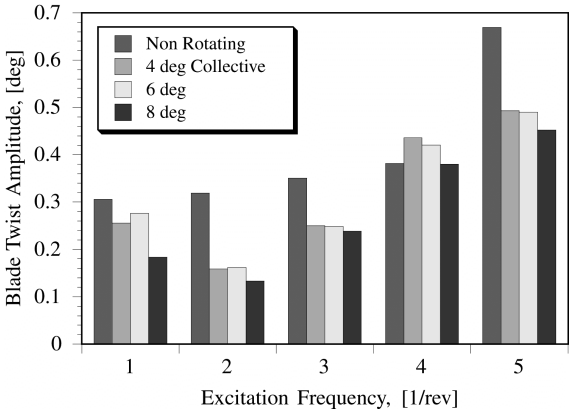

Fig. 38: Hover Test Results, Blade Tip Twist at 875 RPM, Excitation 100 Volts RMS (Clamped Actuator Beam to Blade Tip) [73]

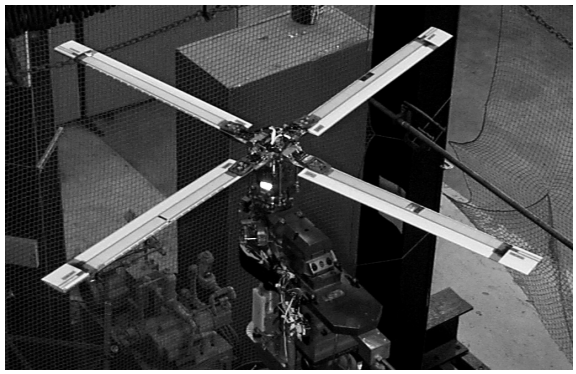

Fig. 39: Active blade tip rotor on the hover test stand, diameter 6 feet, tip Mach .47, RPM 2000, blade tip 10%R, Bell 412 hub.

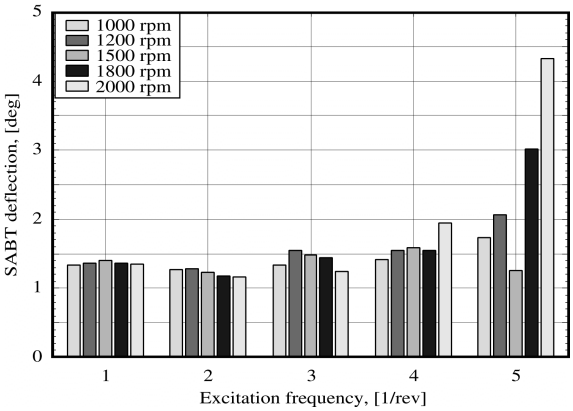

Fig. 40: Active blade tip rotor test in hover: Oscillatory tip amplitude with RPM sweep at 100 V_{rms} and 2 deg collective

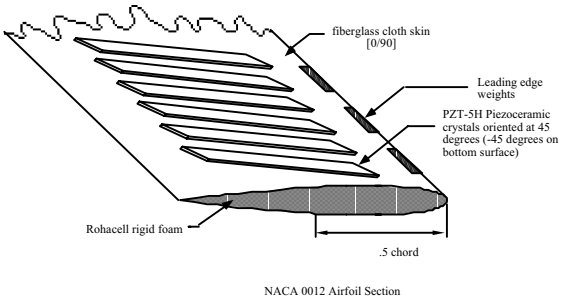

Fig. 41: Piezoceramic Blade Cross Section Details

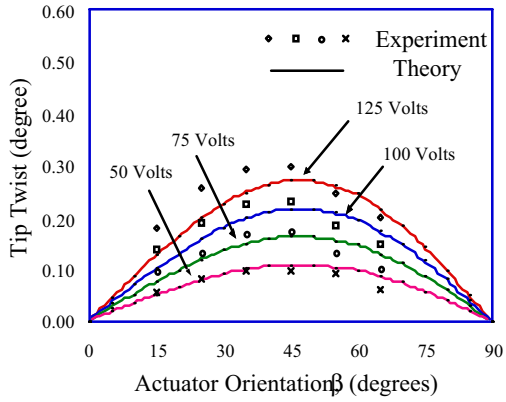

(a) Bond Thickness .020 inch

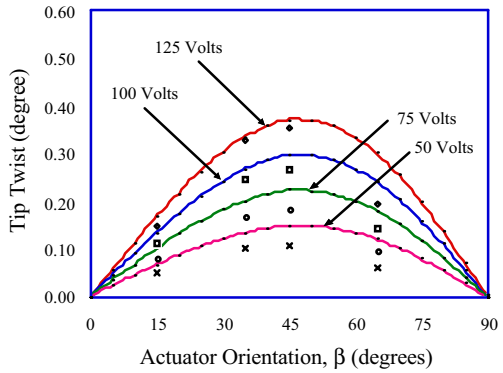

(b) Bond Thickness .010 inch

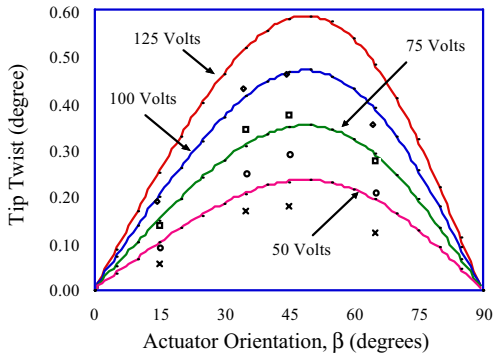

(c) Bond Thickness .0025 inch

Fig. 42: Effect of Bond Thickness and Actuator Orientation on Cantilevered Beam Tip Twist [79]

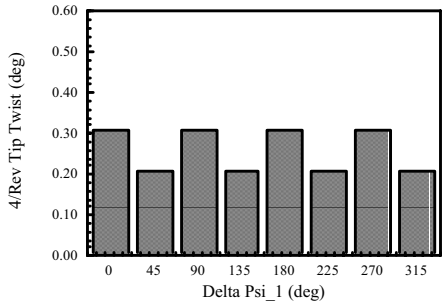

(a) Single-Layer Actuators

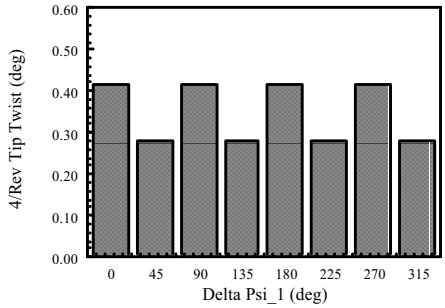

(b) Dual-Layer Actuators

Fig. 43: Blade Response at 4/rev Excitation at 100 Volts RMS in a wind tunnel test at an advance ratio μ=0.33 [80]

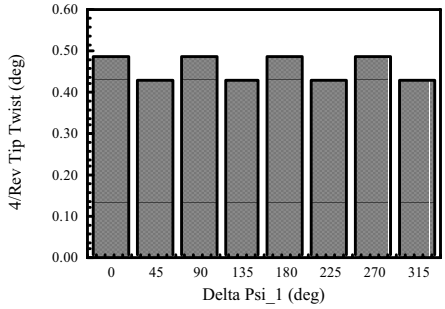

(a) Blade Response at Tip

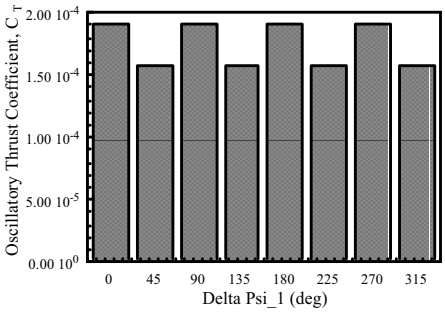

(b) Oscillatory Rotor Thrust

Fig. 44: Dual-Layer Actuators Blade Response at 4/rev Excitation at 150 Volts RMS in a wind tunnel

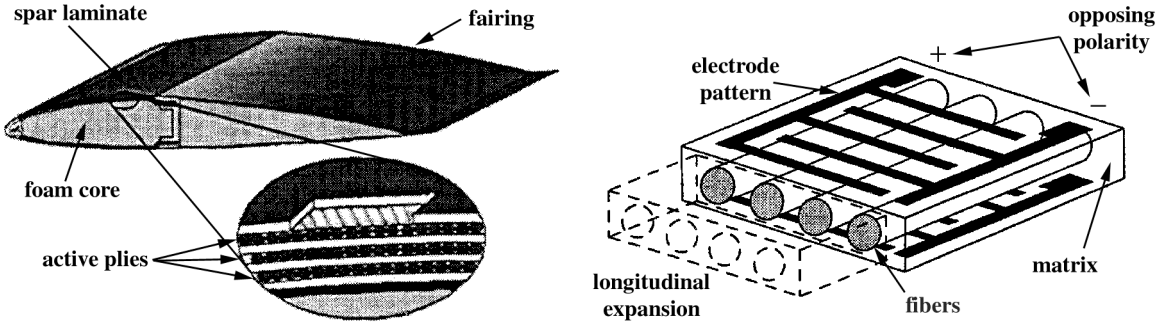

Fig. 45: Active twist blade incorporating active piezo fibers

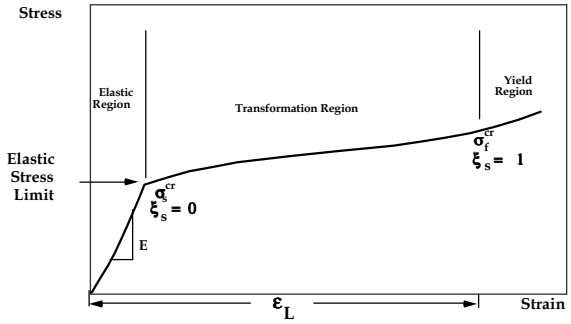

Fig. 46: Schematic diagram of stress-strain characteristics of SMA

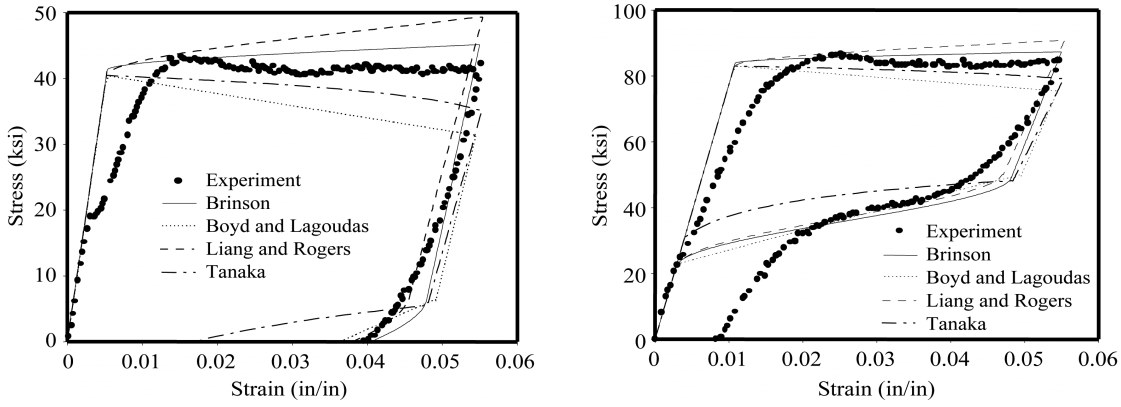

(a) 100^{O}F Temperature (b) 140^{O}F Temperature

Fig. 47: Stress-Strain Curves of 20 mil Nitinol Wire [4]

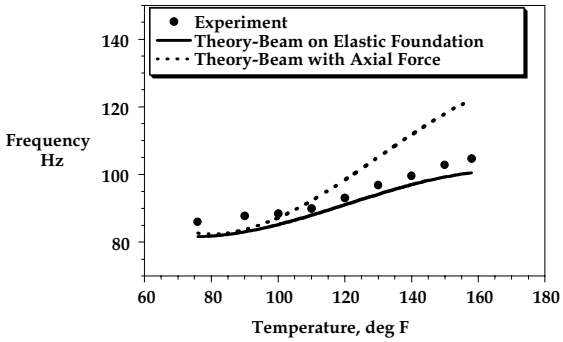

Fig. 48: Fundamental Frequency of Clamped-Clamped Graphite-Epoxy Beam Activated by One 20 mil Dia SMA Wire, Beam Dimensions: length = 18 in., width = 0.25 in., thickness = 0.068 in. [96]

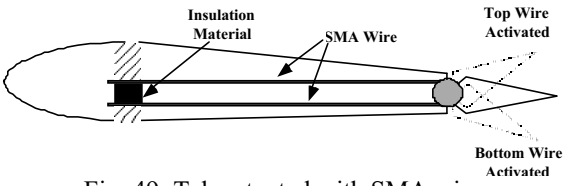

Fig. 49: Tab actuated with SMA wires

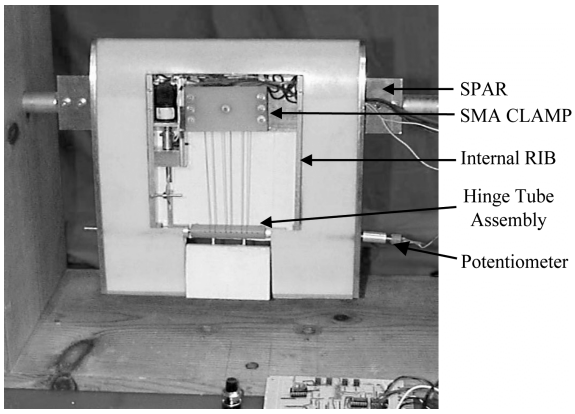

Fig. 50: Blade section with tab actuated with 3 SMA wires

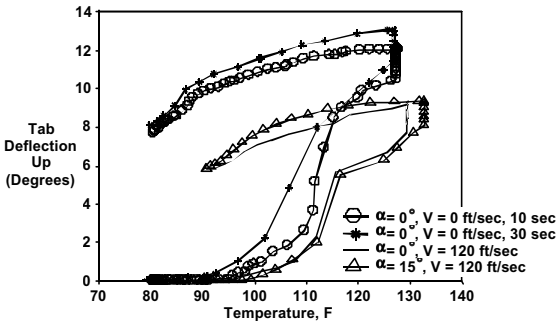

Fig. 51: Comparison of bench-top and open-jet wind tunnel test results for tab deflection at different temperatures [102]

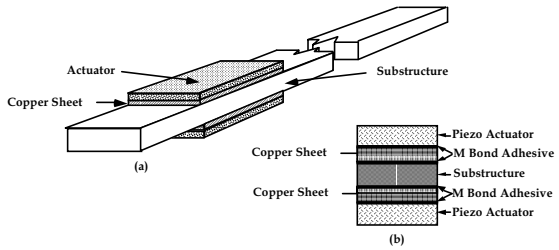

Fig. 52: Solid Beam with Piezoelectric Actuators

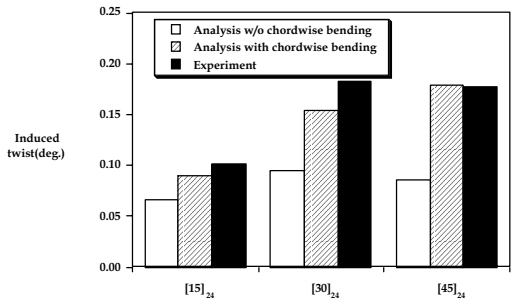

Fig. 53: Induced twist of graphite-epoxy solid beams under piezoactuation, free actuator strain=240 microstrain [103]

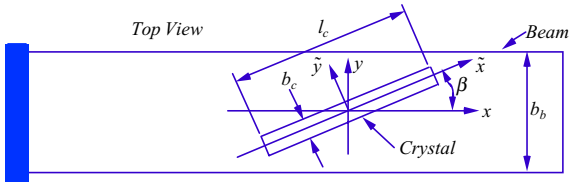

Fig. 54: Piezo element skewed from beam axis

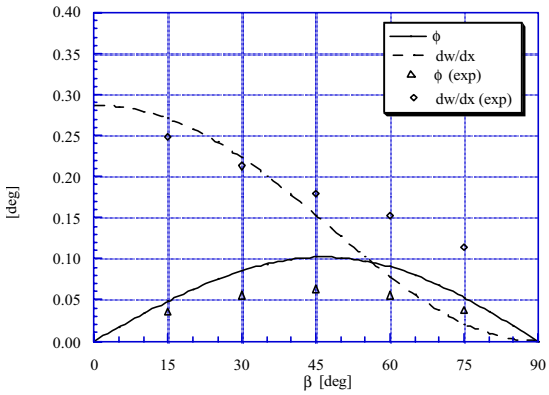

Fig. 55: Bending slope and twist results of a Cantilevered Beam (Tip) [45]